

Kinesin Spindle Protein (KSP) Inhibitors. 9. Discovery of (2*S*)-4-(2,5-Difluorophenyl)-*N*-[(3*R*,4*S*)-3-fluoro-1-methylpiperidin-4-yl]-2-(hydroxymethyl)-*N*-methyl-2-phenyl-2,5-dihydro-1*H*-pyrrole-1-carboxamide (MK-0731) for the Treatment of Taxane-Refractory Cancer

Christopher D. Cox,^{*,‡} Paul J. Coleman,[‡] Michael J. Breslin,[‡] David B. Whitman,[‡] Robert M. Garbaccio,[‡] Mark E. Fraley,[‡] Carolyn A. Buser,^{§,†} Eileen S. Walsh,[§] Kelly Hamilton,[§] Michael D. Schaber,[§] Robert B. Lobell,[§] Weikang Tao,[§] Joseph P. Davide,[§] Ronald E. Diehl,[§] Marc T. Abrams,[§] Vicki J. South,[§] Hans E. Huber,[§] Maricel Torrent,^{||} Thomayant Prueksaritanont,[⊥] Chunze Li,[⊥] Donald E. Slaughter,[⊥] Elizabeth Mahan,[⊥] Carmen Fernandez-Metzler,[⊥] Youwei Yan,[#] Lawrence C. Kuo,[#] Nancy E. Kohl,^{§,†} and George D. Hartman[‡]

Departments of Medicinal Chemistry, Cancer Research, Molecular Systems, Drug Metabolism, and Structural Biology, Merck Research Laboratories, P.O. Box 4, Sumneytown Pike, West Point, Pennsylvania 19486

Received April 4, 2008

Inhibition of kinesin spindle protein (KSP) is a novel mechanism for treatment of cancer with the potential to overcome limitations associated with currently employed cytotoxic agents. Herein, we describe a C2-hydroxymethyl dihydropyrrole KSP inhibitor (**11**) that circumvents hERG channel binding and poor in vivo potency, issues that limited earlier compounds from our program. However, introduction of the C2-hydroxymethyl group caused **11** to be a substrate for cellular efflux by P-glycoprotein (Pgp). Utilizing knowledge garnered from previous KSP inhibitors, we found that β -fluorination modulated the pK_a of the piperidine nitrogen and reduced Pgp efflux, but the resulting compound (**14**) generated a toxic metabolite in vivo. Incorporation of fluorine in a strategic, metabolically benign position by synthesis of an *N*-methyl-3-fluoro-4-(aminomethyl)piperidine urea led to compound **30** that has an optimal in vitro and metabolic profile. Compound **30** (MK-0731) was recently studied in a phase I clinical trial in patients with taxane-refractory solid tumors.

Introduction

Advances in molecular biology and a better understanding of the mechanisms responsible for cancer formation and metastasis have led to a significant shift in focus toward *targeted therapies* for the treatment of neoplastic disease.¹ These efforts have resulted in the recent approval of innovative new drugs that show promise for extending the length and improving the quality of life for cancer patients.² However, cytotoxic agents have been the mainstay of effective chemotherapeutic approaches for the past several decades, and they continue to play an important role in the battle against cancer, both as stand-alone agents and, more recently, as adjuvants with targeted therapies.³ It is therefore not surprising that the development of more effective and better tolerated cytotoxic agents continues to be an area of focus in the pharmaceutical industry.⁴

Many successful cytotoxic agents currently in clinical use, such as the taxanes and *Vinca* alkaloids, operate during mitosis by interfering with the cellular machinery required for cell division and diverting the cell down a pathway of programmed cell death, or apoptosis. As defined by their mechanism of action, these antimitotic agents are *spindle poisons* in that they directly target the mitotic spindle by binding to tubulin, a protein required not only for mitosis but also for structural integrity and proper function of terminally differentiated cells.⁵

To avoid side effects attributed to the nonselective mechanism of action of spindle poisons, recent efforts have been focused on identification of new targets in the mitotic pathway that play a role only in dividing cells, or *targeted antimitotic therapies*.⁶ A leading candidate to emerge from these efforts is kinesin spindle protein (KSP^a or *HsEg5*), a member of the kinesin family of molecular motor proteins. Kinesins bind to tubulin and utilize the energy generated from the hydrolysis of ATP to produce a directed force that can move cargo, regulate microtubule dynamics, or control chromosomal attachment.⁷ KSP is a *mitotic kinesin* that is only expressed in dividing cells and plays a critical role in the formation of a properly organized bipolar mitotic spindle.⁸ Inhibition of KSP function results in mitotic arrest with a characteristic monoaster phenotype and subsequently leads to apoptosis.⁹

KSP inhibitors have several potential advantages over traditional spindle poisons as chemotherapeutic agents. Since their mechanism of action only affects dividing cells, KSP inhibitors are not expected to cause peripheral neuropathy, a side effect attributed to disruption of the tubulin network in neurons and leads to the discontinuation of taxane or *Vinca* alkaloid treatment in some patients.⁶ Additionally, KSP inhibitors can be effective in cancer cells that are refractory to spindle poisons because of overexpression of P-glycoprotein (Pgp) or tubulin mutations.¹⁰ Finally, a water-soluble KSP inhibitor will circumvent the onerous dosing regime employed for taxane administration, a nonaqueous vehicle that requires premedication to prevent vehicle-associated toxicities.^{10b} These promising characteristics have encouraged us, as well as others, to initiate clinical trials

* To whom correspondence should be addressed. Phone: +1-215-652-2411. Fax: +1-215-652-7310. E-mail: chris_cox@merck.com.

[‡] Department of Medicinal Chemistry.

[§] Department of Cancer Research.

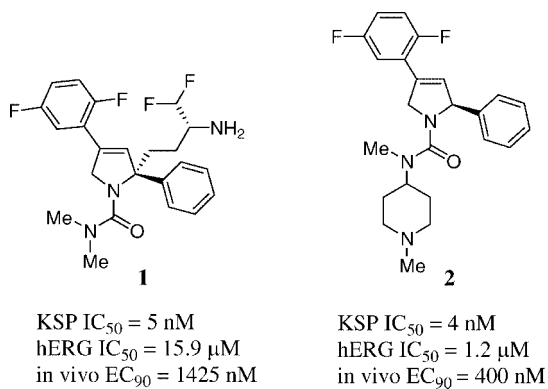
[†] Current address: Department of Oncology Research, Merck Research Laboratories, 33 Avenue Louis Pasteur, Boston, MA 02115.

^{||} Department of Molecular Systems.

[⊥] Department of Drug Metabolism.

[#] Department of Structural Biology.

^a Abbreviations: KSP, kinesin spindle protein; MDR, multidrug resistant; Pgp, P-glycoprotein; hERG, human ether-a-go-go related gene; MTD, maximum-tolerated dose; GI, gastrointestinal.

Chart 1. Previously Reported KSP Inhibitors

to evaluate KSP inhibitors for the treatment of taxane-refractory cancer.^{4,11,12}

In a series of recent publications, we disclosed our research efforts that began with a high-throughput screening (HTS) hit and culminated in the design of potent and selective KSP inhibitors **1** and **2** (Chart 1).¹³ Though these compounds illustrate that synthesis of water-soluble KSP inhibitors with antimetabolic activity in a Pgp-overexpressing cell line is feasible, **1** had poor in vivo activity in a mouse xenograft assay,¹⁴ whereas **2** and related compounds demonstrated unacceptable levels of affinity for the human ether-a-go-go related gene (hERG) channel.^{13b} Herein, we disclose a new series of C2-hydroxymethyl dihydropyrrole KSP inhibitors derived by hybridization of **1** and **2**. This new series overcame the issues associated with our previous compounds and led to a clinical candidate for the treatment of taxane-refractory cancer.

Chemistry

Compounds in the 2,2-disubstituted dihydropyrrole series, including **1**, were synthesized by the route described in Scheme 1. Following formation of the benzylimine of racemic phenylglycine methyl ester (**3**), alkylation with methallyl dichloride under phase transfer conditions provided the mono C-alkylated product (not shown or isolated). The benzylimine was hydrolyzed with aqueous HCl, and during workup, intramolecular N-alkylation occurred to furnish pyrrolidine **4**. The methyl ester of **4** was reduced with LAH to afford an amino alcohol that was treated with 1,1'-carbonyldiimidazole to provide oxazolidinone **5**. Ozonolysis of the exocyclic double bond generated bicyclic ketone **6**. This seven-step sequence can easily be carried out on mole-scale without the need to purify any intermediates and provides crystalline **6** by trituration from acetone in an overall yield of 15% from phenylglycine methyl ester.

The triflate of ketone **6** was formed regioselectively with PhN(Tf)₂ and NaHMDS^{13b} and converted to **7** via Suzuki reaction with commercially available 2,5-difluorophenylboronic acid in 69% yield over two steps. The oxazolidinone ring was hydrolyzed with NaOH, and the resulting amino alcohol protected with *tert*-butyldimethylsilyl chloride provided **8** in 83% yield. As noted in our previous reports, only the (*S*)-antipode of compounds in this class of inhibitors exhibits KSP activity.¹³ Chiral HPLC separation was therefore carried out at this stage to provide optically pure (*S*)-**8**. Treatment with triphosgene, followed by addition of dimethylamine and subsequent deprotection, led to **9** in 78% yield from (*S*)-**8**. Elaboration of the primary alcohol in **9** to functionalized amino

side chains, such as that in **1**, was carried out in a straightforward manner as previously described.^{13d}

Results and Discussion

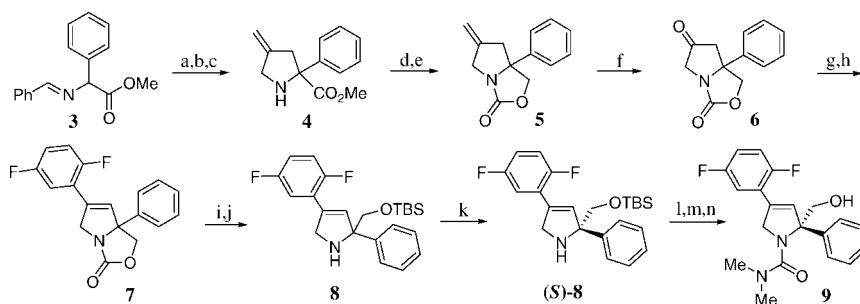
As discussed in the Introduction, though compound **1** possessed an optimized in vitro profile, it displayed poor activity in an in vivo assay designed to measure mitotic arrest in a tumor xenograft (*vide infra*).¹⁴ In an effort concurrent with these studies, we discovered compounds such as **2** wherein the solubilizing basic amine is connected to the dihydropyrrole core through an unsymmetrical urea linkage. These compounds, though more effective than **1** in vivo, demonstrated an unacceptable in vitro profile characterized by high affinity for the hERG channel.^{13b} Blockade of this ion channel has been implicated in drug-induced prolongation of the QT interval of the EEG, an event associated with a potential fatal polymorphic ventricular tachycardia, torsade de pointes.¹⁵

We ultimately discovered that it was possible to overcome the hERG channel binding in compounds related to **2** by reducing the basicity of the amine and restoring water solubility with a phosphate prodrug strategy.¹⁶ Separately, we found that improved in vivo efficacy could be obtained in analogues related to **1** by replacing the dihydropyrrole urea with a dihydropyrazole acetamide.¹⁴ However, at the time of the initial work, we reached an impasse with these two series of compounds and thus began to search for structural alterations that would generate a new series with the potential to overcome the shortcomings of **1** and **2**.

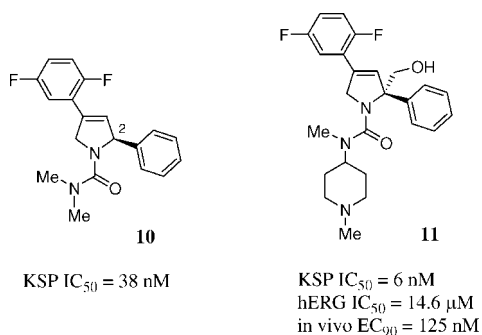
During the synthesis of compounds in the 2,2-disubstituted dihydropyrrole series, we recognized that incorporation of the C2-hydroxymethyl group preserved KSP potency, as revealed by comparison of **9** (KSP IC₅₀ = 78 nM) to the C2-H analogue **10** (KSP IC₅₀ = 38 nM) made earlier in our program (Chart 2).^{13b} Though the potency of **9** was not in the range desired for leading compounds, we were encouraged by the discovery that a small, polar functionality with the potential to significantly alter physical properties is tolerated by KSP. We therefore decided to investigate the effect of C2-hydroxymethylation on the more potent inhibitor **2** and were pleased to find that the resulting compound (**11**) has potency similar to that of **2** in vitro, as well as superior activity in vivo (Chart 2). Most interesting, however, was the order of magnitude decrease in affinity for binding to the hERG channel demonstrated by **11** relative to **2**.

Extensive precedent exists for the circumvention of hERG activity by rational medicinal chemistry design.¹⁷ Among the most successful reported approaches for diminishing binding to the hERG channel are modulation of lipophilicity, as measured by log *P*, and discrete structural modifications that disrupt the putative π -stacking and hydrophobic interactions between the drug candidate and the channel cavity. It is therefore not unexpected that installation of a polar, hydrogen-bond donating functionality at a central position within the core architecture of **11** results in a dramatic effect on hERG binding. The hydroxymethyl group decreased the experimental log *P* from 2.5 in **2** to 1.7 in **11**, and reduced hERG binding is a general trend observed for compounds in this series of C2-hydroxymethyl analogues (*vide infra*).

Although introduction of the hydroxymethyl group had a favorable effect on hERG binding, it negatively impacted the Pgp profile. For example, whereas **2** is not a Pgp substrate, **11** is efficiently effluxed from cells by Pgp as indicated by its multidrug resistance (MDR) ratio, a measure of Pgp-mediated resistance to mitotic arrest that we have recently reported to be a reliable high-throughput approach to measure Pgp susceptibility of KSP inhibitors.^{13d} The MDR ratio is calculated by dividing

Scheme 1^a

^a Reagents and conditions: (a) $\text{ClCH}_2\text{C}(\text{CH}_2)_2\text{CH}_2\text{Cl}$, Bu_4NHSO_4 , 10 M NaOH, DCM; (b) 1 M HCl; (c) $\text{Na}_2\text{CO}_3/\text{H}_2\text{O}$; (d) LAH, THF, 0°C to room temp; (e) CDI, TEA, DCM; (f) O_3 , DCM, -78 °C, then DMS (15% yield from **3**); (g) NaHMDS, THF, -78 °C, then $\text{PhN}(\text{Ti})_2$; (h) 2,5-difluoroboronic acid, Na_2CO_3 , LiCl, $\text{Pd}(\text{PPh}_3)_4$, DME (69% for two steps); (i) 10 M NaOH, EtOH, 60°C; (j) TBSCl, imidazole, 5% DMF in DCM (83% for two steps); (k) Chiralpak AD, 1% *i*-PrOH in hexanes (0.1% DEA as modifier), first isomer to elute is the desired (*S*)-isomer; (l) triphosgene, TEA, THF; (m) NHMe_2 ; (n) HF-TEA, CH_3CN (78% for three steps).

Chart 2. Relevant Properties of KSP Inhibitors **10** and **11**

the IC_{50} for induction of mitotic arrest in a cell line that highly overexpresses Pgp by the IC_{50} in the parental line that does not express Pgp. An MDR ratio of unity indicates that the KSP inhibitor is not effluxed by Pgp because it is equipotent in both cell lines. At the other extreme, paclitaxel [(1*S*,2*S*,3*R*,4*S*,7*R*,9*S*,10*S*,12*R*,15*S*)-4,12-diacetoxy-15-[[[(2*R*,3*S*)-3-(benzoylamino)-2-hydroxy-3-phenylpropanoyl]oxy]-1,9-dihydroxy-10,14,17,17-tetramethyl-11-oxo-6-oxatetracyclo[11.3.1.0~3,10~.0~4,7~]heptadec-13-en-2-yl benzoate] has a ratio of greater than 25 000, since it is devoid of activity in the overexpressing cell line. We considered compounds with a ratio of less than 10 to be acceptable for development, but **11** had a ratio of 21, with an EC_{50} of only 150 nM in the Pgp-overexpressing cell line.¹⁸

Pgp is encoded in the human MDR1 gene and has been extensively studied as a major feature of the multidrug resistant (MDR) phenotype. It plays an important role not only in the resistance of cancer cells to cytotoxic agents such as paclitaxel and the *Vinca* alkaloids but in other aspects of drug design and delivery as well.¹⁹ Extensive efforts in recent years have been directed toward understanding the mechanisms of substrate recognition by Pgp, resulting in a number of models that attempt to explain the SAR of Pgp substrates.²⁰ However, a complete understanding of the specific molecular elements required for recognition is complicated by the unusual promiscuity of Pgp and a lack of generalized assays that allow for direct comparisons between studies from different sources. Several successful efforts to rationally design drug candidates that circumvent Pgp efflux have been reported.²¹ However, the exercise remains mainly an empirical endeavor, albeit one that can be aided by several guiding principles such as increasing passive permeability, reducing molecular size, and removing or weakening hydrogen-bond donors and acceptors. The observation that hydroxymethyl substitution increased Pgp-mediated efflux in progressing from **2** to **11** is consistent with the recently reported

Table 1. Effect of *N*-Alkyl Group on Overall Compound Profile

R	Compound	KSP IC_{50} (nM) ^a	MDR ratio	pK_a ^b	hERG IC_{50} (μM) ^c
H	12	7.4 ± 1.2	345.1	9.8	19.2 ± 1.4
	13	5.1 ± 0.8	29.9	9.1	n.t.
Me	11	6.2 ± 2.9	21.2	8.8	14.6 ± 2.3
	14	5.0 ± 1.4	4.5	7.6	13.8 ± 2.9
	15	5.9 ± 2.1	1.2	7.5	15.2 ± 0.6
	16	34.1 ± 4.5	1.2	4.9	n.t.

^a Average from at least $n = 3$ experiments. ^b Values were determined with a Sirius GLpK_a titrator, average of $n = 3$ determinations. ^c Average from at least $n = 2$ experiments. n.t. = not tested.

finding that hydroxyl substitution at C11 in a series of structurally related glucocorticoids was responsible for enhanced Pgp affinity and cellular efflux.²²

In recent publications, we demonstrated that it is possible to balance Pgp efflux potential (as measured by the MDR ratio) with KSP potency by careful modulation of amine basicity for two related series of KSP inhibitors.^{13d,14} Specifically, we found that by constraining the pK_a to a range of 6.5–8.0, maximal KSP inhibitory activity is maintained, and the ability for the compound to induce mitotic arrest in Pgp-overexpressing cells is optimized. Interestingly, the pK_a of **11** is 8.8, which is consistent with its high MDR ratio. To determine if a similar trend holds for modulating basicity of the piperidine nitrogen, *N*-alkyl analogues of **11** with groups of varying electron-withdrawing ability were prepared and evaluated (Table 1).

As we found for the previous series of KSP inhibitors, a good correlation between optimal profile and pK_a is observed: the inhibitor with $\text{pK}_a < 6.5$ (**16**) has reduced KSP potency, while those inhibitors with $\text{pK}_a > 8$ (**11–13**) lose appreciable activity in Pgp-overexpressing cells, as indicated by high MDR ratios. Notably, all analogues maintained favorable hERG binding profiles. The two inhibitors with a pK_a between 6.5 and 8.0, β -monofluorinated analogue **14** and cyclopropylamine **15**, possessed the optimal balance between KSP potency and MDR ratio and were chosen for further characterization.

Cyclopropyl analogue **15** was found to be a potent time-dependent inhibitor of CYP3A4, a well-known liability of this structural motif,²³ and was not further pursued. In contrast, **14** demonstrated a promising overall profile, including excellent *in vivo* activity ($EC_{90} = 100$ nM), good formulation properties, and the potential for suitable pharmacokinetic parameters. As part of our preclinical evaluation of **14**, we studied dose proportionality in the rat with *iv* bolus doses of 1, 4, and 12 mg/kg. As desired, a linear increase in exposure with dose was observed, with **14** achieving AUC levels of 0.5, 2.5, and 9.5 $\mu\text{M h}^{-1}$, respectively; however, we were surprised to find mortality within 12 h postdose in 2 of 3 rats in the 12 mg/kg group.

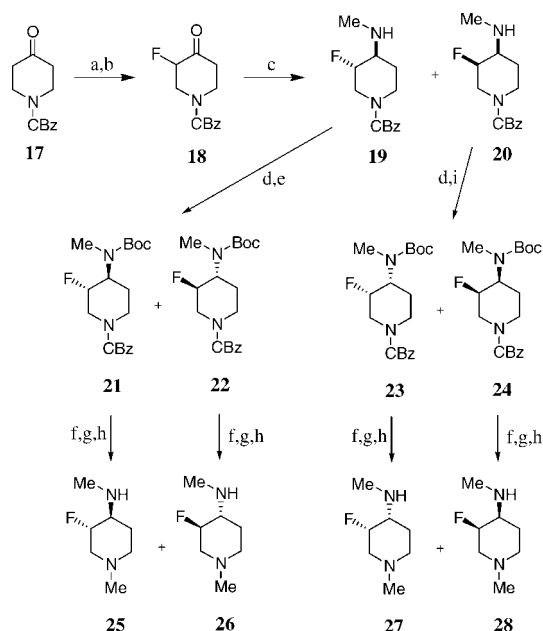
Acute toxicity is not an expected mechanism-based effect for inhibition of KSP and has not been observed in our preclinical program with any compound other than **14**. The dose-limiting, mechanism-based toxicity observed for KSP inhibitors both preclinically and in humans is neutropenia (depletion of white blood cells) and typically manifests in 4–10 days following compound administration.¹¹ In our search for a compound-specific source of toxicity, we identified the fluoroethylamine of **14** as a potential liability. If N-dealkylation of the piperidine ring were to occur *in vivo*, a likely byproduct would be fluoroacetate, a known toxin with acute pharmacology.²⁴ In fact, we discovered that N-dealkylated analogue **12** is the major metabolite generated in rat liver microsome and hepatocyte incubations, suggesting that formation of fluoroacetate is indeed the source of toxicity *in vivo*.

Since **14** demonstrated the profile desired in a clinical candidate, we began a search for isoelectronic replacements of the fluoroethyl substituent that would maintain the overall properties of **14** and not impart toxicity *in vivo*. The most prudent choice was installation of fluorine directly on the piperidine ring. This strategy eliminates the possibility of forming a low molecular weight fluorinated acid as a metabolic byproduct and also provides the opportunity to carefully tune the pK_a of the piperidine nitrogen by controlling relative stereochemistry of the fluorine substituent. It has been shown that an axial 3-fluoro substituent lowers the pK_a of a piperidine nitrogen by approximately 1 log unit, whereas an equatorial 3-fluoro can lower the pK_a by nearly 2 units, a tactic that was employed in an effort to generate 5-HT_{1D} receptor agonists with improved pharmacokinetic profiles.²⁵ We thus turned our attention to synthesis of the required stereodefined fluorinated piperidine analogues to investigate this strategy.

Utilizing a variant of the route reported by van Niel,²⁵ we synthesized the four enantiomerically pure *N*-methyl-3-fluoro-4-(aminomethyl)piperidine analogues as shown in Scheme 2. Formation of the TMS enolate of the protected 4-ketopiperidine **17**, followed by electrophilic fluorination with Selectfluor, afforded α -fluoroketone **18** in 90% yield. Reductive amination of **18** with methylamine in MeOH provided a separable mixture of trans and cis isomers **19** and **20** in a combined yield of 62%. The isomers were processed separately, beginning with Boc protection of the secondary amine, followed by resolution of the enantiomers with chiral stationary phase HPLC. Removal of the CBz group by transfer hydrogenation, reductive amination with formaldehyde, and Boc removal provided the four enantiomerically pure *N*-methyl-3-fluoro-4-(aminomethyl)piperidine analogues **25–28**.

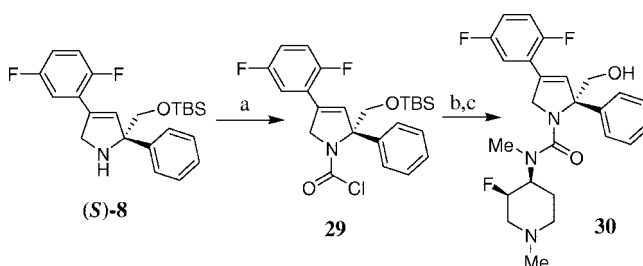
The four isomers were coupled to the dihydropyrrrole core as illustrated in Scheme 3 using enantiomerically pure *cis*-fluoropiperidine **28** as an example. Carbamoyl chloride **29** was first generated by treatment of (*S*)-**8** with triphosgene and triethylamine in THF. This intermediate was easily isolated in

Scheme 2^a



^a Reagents and conditions: (a) TMSCl, TEA, DMF, 80°C; (b) Selectfluor, CH₃CN, 0°C (90% for two steps); (c) MeNH₂, AcOH, NaBH₃CN, MeOH (1.3:1 ratio of 19:20, 62% combined yield); (d) Boc₂O, TEA, CH₂Cl₂; (e) Chiralpak AD, 15% IPA/hexanes (45% yield of **21** and 49% of **22** from **19**); (f) 1,4-cyclohexadiene, 10% Pd/C, EtOH; (g) CH₂O, AcOH, NaBH₃CN, MeOH; (h) HCl(g), EtOAc, workup with Na₂CO₃ (>90% yield for three steps); (i) Chiralpak AD, 20% IPA/hexanes (45% yield of **23** and 41% of **24** from **20**).

Scheme 3^a

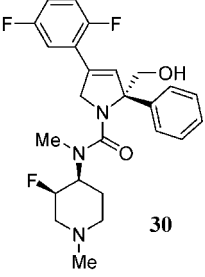
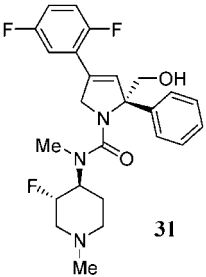


^a Reagents and conditions: (a) triphosgene, TEA, THF, 0°C (100%); (b) **28**, TEA, DMAP, THF; (c) TEA–HF, CH₃CN, 37°C (63% yield over two steps).

quantitative yield and is stable for months when stored in the freezer. Reaction of **29** with fluoropiperidine **28** provided **30** following removal of the TBS protecting group. Synthesis of the other three fluoropiperidine analogues was carried out by an analogous route with **25–27** to provide all four optically and diastereomerically pure isomers. The more potent *cis* isomer (**30**) and *trans* isomer (**31**) are shown in Table 2.²⁶

Because of the larger *A*-value of the amino group relative to fluorine, the urea substituent is expected to occupy the equatorial position of the piperidine ring, placing the fluorine axial in *cis* analogue **30** and equatorial in *trans* analogue **31**. This conjecture was subsequently confirmed by X-ray analysis (*vide infra*). As expected from precedent, the equatorial fluorine has a dramatic effect on pK_a , lowering it from 8.8 in nonfluorinated analogue **11** to 6.6 in **31** (Table 2). On the other hand, the axial fluorine results in a more modest effect on basicity, affording a pK_a of 7.6 in **30**. Compound **30** displayed superior potency in both the enzymatic KSP assay and a cell-based assay relative to **31**, and both compounds displayed little affinity for binding to the hERG channel. Importantly and consistent with its favorable pK_a , **30** also

Table 2. Effect of Fluorine Stereochemistry on Compound Profile^a

	axial	equatorial
fluorine disposition		
		
		
pK _a ^b	7.6	6.6
KSP IC ₅₀ (nM)	2.2 ± 1.2	11.5 ± 6.1
Cell EC ₅₀ (nM)	5.3 ± 2.3	16.5 ^c
MDR ratio	4.5	2.4
hERG IC ₅₀ (μM)	20.5 ± 1.7	36.9 ^c

^a Average from at least $n = 3$ experiments, unless otherwise noted. ^b Values were determined with a Sirius GLpK_a titrator, average of $n = 3$ determinations. ^c Value is from $n = 1$ determination.

has significant activity in Pgp-overexpressing cells, with potencies of 4.2 and 18.9 nM in the parental and Pgp-overexpressing cell lines, respectively, resulting in an MDR ratio of 4.5. For comparison, the corresponding values for paclitaxel are 0.5 nM and >10 μM. Thus, **30** has the ability to induce a mitotic block with an IC₅₀ of 19 nM in cells that are refractory to paclitaxel due to Pgp-overexpression. On the basis of a favorable overall in vitro profile, **30** was selected for in vivo evaluation.

The primary in vivo assay employed during lead optimization was a pharmacodynamic assay to determine mitotic arrest in tumors from nude mice bearing an A2780 human ovarian carcinoma xenograft. The minimum plasma concentration required to induce the maximum extent of mitotic arrest in the tumor is defined as the EC₉₀ for in vivo activity. We assessed mitotic arrest by determining the phosphorylation state of histone H3 on Ser-10, a residue that is phosphorylated exclusively in mitosis by the Aurora kinases,²⁷ and quantitated the results by immunohistochemical staining of resected tumors. For compound administration, subcutaneously implanted Alzet osmotic pumps were used for their ability to mimic a continuous iv infusion over the 22 h course of the experiment. We envision employing a continuous iv infusion in the clinic because mitotic arrest induced by KSP inhibition must be maintained for a minimum of 16–24 h to induce the apoptotic response.²⁸ This protocol provides the best opportunity to maintain plasma exposure for the required length of time without exposing the patient to high levels of drug following a bolus infusion.

For the in vivo study, aqueous solutions of **30** were administered to A2780-xenografted mice via minipump at doses of 2.5, 5, 10, 20, and 40 (mg/kg)/day. As illustrated in Figure 1, **30** exhibited a dose-proportional increase in both exposure and mitotic arrest in tumors, and the maximal level of mitotic block (EC₉₀) occurred at a minimum plasma level of 94 nM from the 10 (mg/kg)/day dose. The degree of maximal mitotic arrest induced by **30** was similar to that of a historical KSP inhibitor that served as a positive control. Subsequent studies in a large cohort of nonxenografted mice revealed that the maximum-tolerated dose (MTD) of **30** when administered via minipump is 12 mg/kg over the course of 24 h.²⁹ Thus, **30** provides a maximal pharmacodynamic effect in tumors at its MTD in our in vivo assay.³⁰

From a retrospective analysis, we believe that the superior in vivo activity of compounds in the C2-hydroxymethyl series, such as **11**, **14**, and **30**, is reflected by the combination of

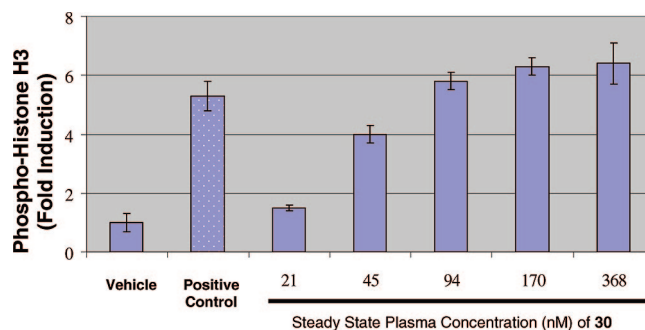


Figure 1. Induction of mitotic block by **30** in tumors from a mouse xenograft assay at doses of 2.5, 5, 10, 20, and 40 (mg/kg)/day. Levels of phosphohistone H3 were measured in the tumor 22 h postdose and plotted relative to vehicle and a known KSPi positive control. Steady-state plasma concentrations were determined at the time of sacrifice by cardiac puncture and also showed a dose dependent increase.

Table 3. Correlation between Cell Potency, Serum Shift, and in Vivo Efficacy^a

compd	KSP IC ₅₀ (nM)	cell EC ₅₀ (nM)	KSP + serum IC ₅₀ (nM) ^b	in vivo EC ₉₀ (nM)
1	5.2 × 0.8	22.5 ± 5.6	84.2 ± 6.0 ^c	1425
11	6.2 ± 2.9	5.6 ± 1.3	29.1 ± 6.5	125
14	5.0 ± 1.4	4.8 ± 0.8	38.8 ± 19	100
30	2.2 ± 1.2	5.3 ± 2.3	29.1 ± 12.2 ^c	94

^a Average from at least $n = 3$ experiments, unless otherwise noted. ^b KSP assay run in the presence of 30% mouse serum. ^c Value is from $n = 2$ determinations.

increased potency in both cell-based and serum-shifted biochemical KSP assays relative to **1**. As illustrated in Table 3, key compounds in the C2-hydroxymethyl series are approximately 4-fold more potent in the cell-based assay and 2- to 3-fold more potent in the KSP assay in the presence of 30% mouse serum. A similar explanation of improved in vivo potency holds across other series of KSP inhibitors recently reported from our group.³¹

On the basis of the ability of **30** to induce mitotic arrest in tumors in vivo, we were encouraged to test its antitumor efficacy in xenograft models. In the clinic, cytotoxic chemotherapeutic agents are typically administered at their MTD on schedules designed to accommodate the induction and recovery from mechanism-based hematopoietic and gastrointestinal (GI) toxicities.^{4a} Typical regimes are once every 3 weeks, once weekly for 3 weeks, or once daily for 5 consecutive days. Thus,

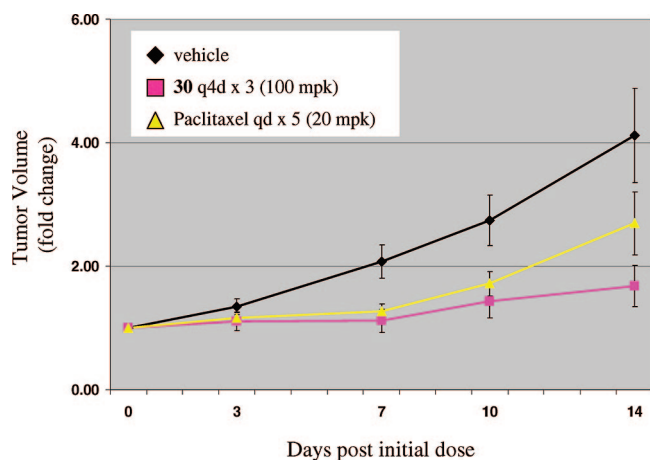


Figure 2. Inhibition of A2780 tumor growth in mice. Both paclitaxel and **30** were dosed at their MTD on the schedule indicated. The data are plotted as the change in tumor volume relative to its starting volume, versus days following initial dose.

we wanted to test dosing protocols in our preclinical model that mimic these likely clinical schedules.

First, studies were undertaken in naive mice to determine the MTD of **30** in protocols that varied the dose, vehicle, and frequency of administration, monitoring survival as an end point. In all cases of lethality following administration of **30**, death is observed at least 6 days after the start of dosing, suggesting that mechanism-based toxicity in hematopoietic and/or GI tissues is the causative factor. To provide support for this hypothesis, peripheral blood counts were determined during these studies to assess the myelosuppressive activity of **30**. Of the different blood cells, neutrophils are most strikingly and consistently depleted, with a nadir in counts on day 4 postdose and recovery to greater than predose levels by day 11 in surviving animals. The severity of neutrophil depletion is directly related to the dose of **30** and suggests that neutropenia may be the dose-limiting toxicity in mice.

Over the course of a large number of experiments, we found that the schedule for administration of **30** that consistently provided the best efficacy is a q4d \times 3 regime, where the MTD of **30** is 100 mpk in pH 4 saline given subcutaneously.³² As indicated in Figure 2, **30** produced statistically significant inhibition of A2780 tumor growth under these conditions. In this experiment, the efficacy of **30** appears statistically superior to that of paclitaxel when given on its optimal schedule of qd \times 5 at 20 mpk ip.

To further our understanding of the potential for **30** to treat refractory tumors, we developed xenograft models utilizing paclitaxel-resistant cell lines. For this purpose, we choose the PTX10 cell line that carries a tubulin mutation at the taxane binding site,³³ as well as the Pgp-overexpressing KB-v cell line utilized in our assay to determine MDR ratio. In order to provide a direct comparison of the *in vivo* efficacy of **30** and paclitaxel from the same study, we designed the assay as a dual flank xenograft model, wherein animals were implanted on contralateral flanks with both a taxane-sensitive cell line (A2780 or KB-3-1) and a taxane-resistant cell line (PTX10 or KB-v).

As pictured in Figure 3, **30** maintains excellent efficacy against the paclitaxel-resistant PTX10 cell line that carries a tubulin mutation at the taxane binding site. In contrast, paclitaxel treatment produces no growth inhibition relative to vehicle in these tumors. Notably, the tumor growth inhibition pictured in Figures 2 and 3 was obtained from the same animals in dual flank mode. In a similar vein, we were able to show that **30**

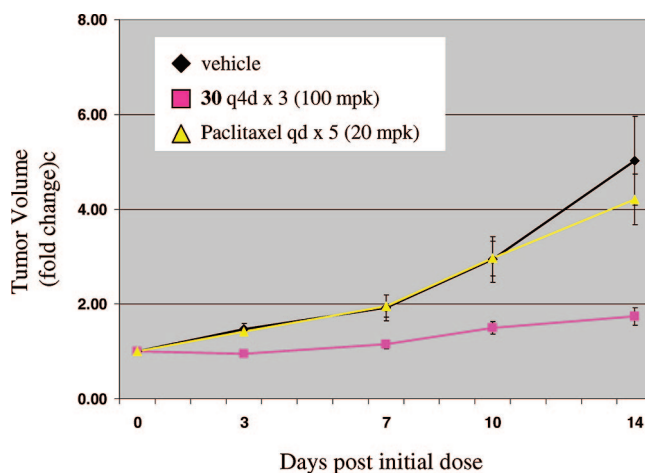


Figure 3. Inhibition of growth in PTX10 tumors that are paclitaxel-resistant because of a tubulin mutation. Both paclitaxel and **30** were dosed at their MTD on the schedule indicated. The data are plotted as the change in tumor volume relative to its starting volume, versus days following initial dose.

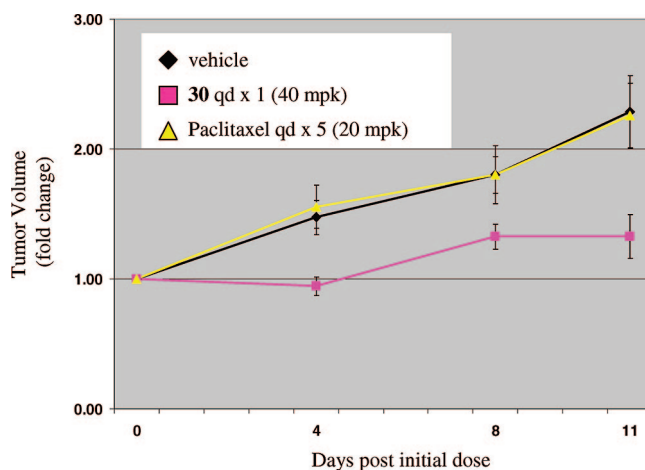


Figure 4. Inhibition of growth in KB-v tumors that are paclitaxel-resistant because of Pgp overexpression. Both paclitaxel and **30** were dosed at their MTD on the schedule indicated. The data are plotted as the change in tumor volume relative to its starting volume, versus days following initial dose.

inhibits the growth of KB-v tumors that highly overexpress Pgp, whereas paclitaxel has no effect (Figure 4).³⁴ Thus, **30** provides significant antitumor efficacy at its MTD in a mouse xenograft assay and is efficacious in tumors that are resistant to paclitaxel because of either tubulin mutation or Pgp overexpression.

Studies were carried out with **30** to confirm that no undesired changes in overall profile or mechanism of action occurred during our lead optimization process. First, we determined that inhibition of KSP by **30** is not competitive with either ATP or microtubules. We also found that **30** is >20000-fold selective for KSP over a panel of eight structurally and functionally related kinesins (CENP-E, MKLP-1, Kif3A, Kif1B, uKHC, nKHC, KIF14, and MCAK; IC₅₀ > 50 μ M in every case). These mechanistic observations suggest that **30** binds in the *induced-fit* allosteric site previously defined by our group.³⁵ This mode of binding nicely explains not only the lack of competition with microtubules and ATP but also the selectivity of **30** for KSP over other kinesins, since the binding site is adjacent to the L5 loop that is unique to the motor domain of KSP. Binding in this allosteric site has subsequently been confirmed for a number of structurally diverse KSP inhibitors, though several recent

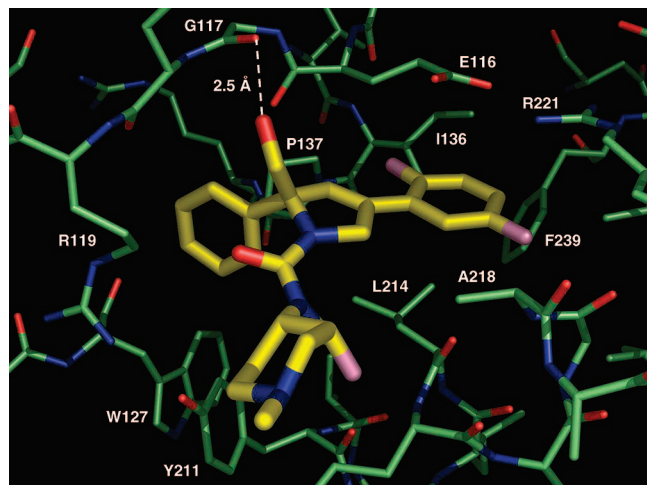


Figure 5. X-ray structure of the active site of the KSP–**30**–ADP ternary complex.

reports have identified ATP-competitive inhibitors that bind to the nucleotide binding site.³⁶

The X-ray structure of the KSP–**30**–ADP ternary complex was determined to 2.3 Å resolution and confirms that **30** does indeed bind in the allosteric site of KSP (Figure 5).³⁷ Also of note is the conformation of the piperidine ring, wherein the fluorine is axial and the urea substituent occupies the equatorial position, as expected.

Three general features present in the KSP–**30**–ADP ternary complex have been identified in progenitor compounds:¹³ (1) the difluorophenyl moiety of **30** occupies a large, hydrophobic area of the allosteric binding site (eastern pocket) made up of lipophilic residues L214, A218, F239, and I136; (2) the unsubstituted phenyl ring of **30** sits orthogonal to the core in a second, smaller region (western pocket) sandwiched between residue P137 (back) and the alkyl side chain of R119 (front); (3) the polar *N*-methyl-3-fluoro-4-(aminomethyl)piperidine moiety of **30** extends toward the solvent-exposed region located above the W127/Y211 π -stacking interaction that seals the protein cavity. The unique and most interesting interaction is the 2.5 Å hydrogen bond formed between the C2-hydroxymethyl group and the backbone carbonyl oxygen of residue G117 located at the roof of the cavity. The G117 carbonyl is the same functionality responsible for hydrogen-bonding to the side chain propylamino group of structures such as **1**.^{13c} Few polar regions are present in the allosteric binding site of KSP, and the hydroxymethyl group in **30** provides an optimal way to utilize the polarity offered by the G117 carbonyl without compromising any of the favorable hydrophobic interactions present in the previously investigated structural series.

Compound **30** also behaves as expected in several assays that, collectively, strongly suggest that KSP inhibition is the mechanism of mitotic arrest and antitumor efficacy. Unlike taxanes and the epothilones, **30** has no effect on microtubule polymerization in vitro at 20 μ M. Additionally, a cell-based assay measuring caspase-3 activation indicates that **30** induces apoptosis in A2780 cells with an EC₅₀ of 2.7 nM. Finally, monoaster formation, the phenotype characteristic of KSP inhibition, occurs in ~90% of A2780 cells following a 16 h incubation with 50 nM of **30** (Figure 6).

Importantly, the physical properties and pharmacokinetic profile of **30** are consistent with that desired for a development compound. The free-base of **30** is a crystalline solid that is stable for 4 weeks at 80 °C open to air. The aqueous solubility of **30**

is >50 mg/mL at pH 4.3, and if kept below room temperature, it has sufficient stability under these conditions to provide an acceptable clinical formulation. The metabolism and pharmacokinetic properties of **30** were studied in three preclinical species, and as illustrated in Table 4, moderate-to-high plasma clearance with a half-life of 1–2 h was observed. The metabolic turnover of **30** is more rapid in animal liver microsomes and hepatocytes than in human, and all metabolites detected in human preparations are found in preclinical species. On the basis of a metabolic scaling method, **30** is predicted to be a low-to-moderate clearance compound in humans (1.4–7 (mL/min)/kg) with a half-life of 2–10 h. These parameters are supportive of continuous iv infusion in man.

The overall safety profile of **30** is also acceptable for an antimitotic agent. Unlike **14**, no acute toxicity is observed in the rat with an iv bolus dose of 15 mg/kg (9.6 μ M h⁻¹), and **30** demonstrates >3000-fold selectivity for KSP over a panel of 160 enzymes, receptors, and transporters in a Panlabs screen at MDS Pharma. Gratifyingly, no QT interval prolongation was seen in preclinical cardiovascular safety studies, consistent with the optimized hERG profile achieved during the discovery effort. On the basis of its favorable efficacy, pharmacokinetic, and safety profile, **30** (MK-0731) was accepted for development and advanced into clinical trials.³⁸

In a phase I open-label clinical trial to test safety and pharmacokinetic parameters in patients with taxane-refractory tumors, **30** was well-tolerated and exhibited dose-proportional exposure following a 24 h continuous infusion. As predicted, **30** is a low clearance compound (100–250 mL/min on average) with a half-life of 4–10 h in humans. At the MTD of 17 (mg/m²)/day every 21 days, **30** was well-tolerated with the anticipated dose-limiting toxicity of neutropenia.³⁸

Conclusion

We demonstrated herein that installation of a hydroxymethyl group at C2 of the dihydropyrrole core provided **11**, which had an optimized hERG profile relative to its progenitor, **2**. However, this change also engendered Pgp susceptibility. By carefully modulating the pK_a of the basic amine in **11**, we discovered fluoroethylated KSPi **14**, which had an optimal in vitro profile but was acutely toxic in vivo. Placement of the fluorine in a strategic, metabolically benign location on the piperidine ring allowed us to simultaneously avoid toxic metabolite formation and tune the pK_a of the nitrogen to provide **30** with an optimized in vitro and in vivo profile. In mouse xenograft assays, **30** induced dose-dependent mitotic arrest in tumors and inhibited tumor growth comparable to paclitaxel. Compound **30** also inhibited tumor growth in cell lines that are resistant to paclitaxel because of either tubulin mutations or Pgp-overexpression. The overall safety and pharmacokinetic profile supports the use of **30** for the treatment of cancer via continuous iv infusion. In clinical trials, **30** exhibits low systemic clearance and is well-tolerated at its MTD, resulting in the expected dose-limiting toxicity of neutropenia.

Experimental Section

(A) Biology. All animal studies were performed according to the NIH Guide for the Care and Use of Laboratory Animals, and experimental protocols were reviewed by the Merck Animal Care and Use Committee.

KSP ATPase Assay. The primary assay for KSP activity is based on a colorimetric determination of inorganic phosphate released from ATP. The KSP motor domain (1–367) was expressed in bacteria with a His₆ tag for purification. Microtubules are polymerized from tubulin at 37 °C, in the presence of 1 mM GTP and 10

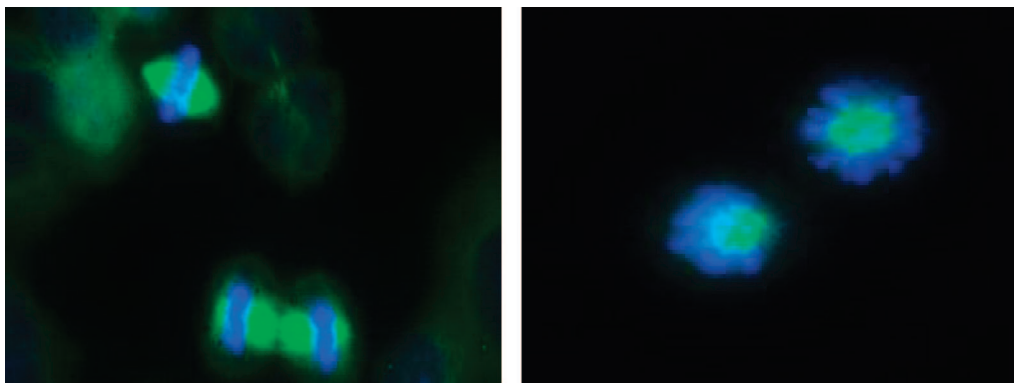


Figure 6. Immunofluorescence pictures of A2780 ovarian carcinoma cells treated with vehicle (left) or 50 nM of **30** (right) for 16 h (blue = DNA, green = microtubules). In the vehicle control image, cells in interphase, metaphase, and anaphase/telophase are visible.

Table 4. Pharmacokinetics of **30** in Preclinical Species^a

species	iv dose	Cl ((mL/min)/kg)	V_{dss} (L/kg)	$T_{1/2}$ (h)
rat	1	66.7 ± 12	3.0 ± 0.6	1 ± 0.1
dog	0.4	15.1 ± 6.4	1.6 ± 0.8	2 ± 0.2
rhesus	0.4	23.1 ± 6.4	2.3 ± 0.4	1 ± 0.3

^a Values are mean ± SD, $n = 3$.

μM paclitaxel, and are then separated from unpolymerized tubulin by centrifugation. Assays were performed in a 96-well plate, with each well containing 4 μL of a DMSO solution of test compound. Compounds were tested as an 11-point titration series, with 3-fold dilutions between each step, ranging from a concentration of 2 μM (in assay) to 34 pM. The reaction was started by adding 156 μL of the reaction buffer to each well; final reaction conditions were 80 mM K-HEPES (pH 6.8), 40 mM KCl, 1 mM EGTA, 0.01% BSA, 1 mM DTT, 2 mM MgCl₂, 1 mM ATP, 0.5 μM tubulin (as polymerized microtubules), 2.5% DMSO, and 0.25 nM KSP. After incubation at room temperature for 3 h, reactions were quenched by addition of 240 μL /well of a solution containing 65 $\mu\text{g}/\text{mL}$ quinaldine red, 0.093% polyvinyl alcohol, and 4.1 mM ammonium molybdate in 0.38 M sulfuric acid. After 5 min for color development, plates were read for optical absorbance at 540 nm. A serum-shifted assay was also run on selected compounds and was performed similarly. Serum was prepared for the assay by extensive dialysis against the primary reaction buffer, using dialysis membranes with a 12–14 kDa cutoff.

KSP ATPase Selectivity. Other kinesins assayed were isolated motor domains, cloned from the corresponding human sequences, and expressed and purified similarly to the procedure used for KSP (CENP-E:1–340, uKHC:1–337, nKHC:1–340, Kif1B:1–350, Kif3A:1–350, MKLP-1:1–435, Kif14:342–720). MCAK motor domain was purchased from Cytoskeleton. Assays were run similarly to the KSP assay described above except that 1 μL of **30** in DMSO was placed in a well to which 39 μL of reaction buffer was added. The reaction buffer used here was identical to that described above except that the tubulin concentration was 1 μM . After 50 min of incubation at room temperature, reactions were quenched by the addition of 40 μL of a solution containing 50 mM EDTA and 1.8 M KCl. Reactions were visualized by the addition of 120 μL of the quinaldine reagent described above. Compound **30** was tested at 50 and 5 μM . Enzyme concentrations varied depending on the enzyme tested: CENP-E, 5 nM; uKHC, 1.5 nM; nKHC, 10 nM; Kif1B, 5 nM; Kif3A, 2 nM; MKLP1, 50 nM; Kif14, 50 nM; MCAK, 50 nM. Compound **30** displayed an $\text{IC}_{50} > 50 \mu\text{M}$ against each kinesin tested.

Kinetic Competition Studies. Assays used a method similar to that described for the primary KSP ATPase assay, with the exception that both ATP and microtubule concentrations varied. Compound **30** was tested at eight different concentrations, including a no compound control, from 0 to 12.5 nM. Either ATP or microtubules were varied independently from the compound over 12 different concentrations; ATP was varied from 10 to 400 μM , while microtubules were varied from 100 to 4000 nM. When ATP

was varied, microtubule concentrations were fixed at 1 μM . When microtubules were varied, ATP concentration was fixed at 1 mM. The enzyme concentration tested was 0.5 nM. Reactions for each condition were initiated in a total volume of 700 μL . Eighty (80) μL aliquots were quenched by addition of an equal volume of a solution containing 50 mM EDTA and 1.8 M KCl at 4, 8, 14, 22, 30, 40, 55, and 70 min and held on ice. Phosphate was detected by addition of 240 μL of the quinaldine red reagent and incubated for 25 min before reading the absorbance at 540 nm. The data were first analyzed as a function of time to derive linear rates for each reaction condition. The velocity data were then analyzed with respect to the Michaelis–Menten or MM fit equation describing mixed inhibition using a nonlinear least-squares method. The data were also analyzed using an alternative model, which incorporates a correction for the reduction in compound concentration in the assay by the enzyme, as a function of enzyme concentration. This model gave essentially identical results to the Michaelis–Menten fit, indicating compound **30** is not competitive with either ATP or microtubules.

Cell-Based Assay. Mitotic arrest was measured by assessing the mitosis-specific phosphorylation of nucleolin using an antibody-coated, bead-based assay. In this assay, total nucleolin is captured on a streptavidin-coated paramagnetic bead coupled with biotinylated nucleolin monoclonal IgG1 antibody 4E2 (Research Diagnostics, Inc.). Nucleolin phosphorylation is detected by an antibody complex consisting of a phospho-specific nucleolin IgM monoclonal antibody, TG3 (Applied NeuroSolutions, Inc.) and a goat antimouse IgM labeled with a ruthenium Tris-bipyridyl complex (BV-TAG Technology, BioVeris Corp.). A2780 cells were seeded at 10 000 cells/well in 96-well plates and grown overnight. Cells were treated in triplicate with vehicle (DMSO) or test compound for 16 h. The final concentration of compound in the assay ranged from 300 to 0.3 nM in a 7-point, half-log dilution series, and the final DMSO concentration was 0.1% v/v. Cells were incubated with compound for 16 h, and then plates of cells were centrifuged at 1500 rpm for 5 min to collect floating cells, followed by lysis via shaking at 4 °C for 20 min in RIPA buffer (50 μL /well) that contained a complete set of protease inhibitors, 1 $\mu\text{L}/\text{mL}$ DNase I, 1.0 mM sodium orthovanadate, and 1.0 μM microcystin. The following procedures were all done at room temperature. Streptavidin-coated paramagnetic Dynabeads (10 $\mu\text{g}/\text{well}$) were premixed with biotinylated 4E2 antinucleolin antibody (50 ng/well) in the assay buffer (pH 7.3 phosphate buffered saline, 1% BSA, and 0.5% Tween-20). The cell lysates (25 $\mu\text{L}/\text{well}$) were subsequently incubated with the premixed beads/4E2 antibody (25 $\mu\text{L}/\text{well}$) in 96-well plates by shaking for 30 min. The antiphosphonucleolin TG3 antibody was then added (50 ng/well), followed by shaking for another 30 min. Finally, a ruthenylated goat antimouse antibody (prepared immediately before use) was added (6 ng/well) and mixed by shaking plates for 2.5 h. The sample plates were read on an IGEN M-series M8 analyzer.

Tubulin Polymerization Assay. Tubulin polymerization was monitored using the light-scattering properties of polymerized

microtubules. The assay was carried out in a 96 well plate, using tubulin at a final concentration of 2.5 mg/mL, with 0.5 mM GTP, in a buffer of 80 mM K-PIPES, pH 6.8, 1 mM MgCl₂, 1 mM EGTA. Compound **30** in DMSO (2 μ L, final concentration of 20 μ M) was added to 198 μ L of reaction buffer, and the mixture was incubated at 37 °C. The optical density was measured at 320 and 340 nm every 30 s for 75 min. Assay plates contained controls for microtubule stabilization (paclitaxel, 20 μ M) and inhibition of polymerization (colchicine, 20 μ M).

Monoaster Formation. The formation of monoastal spindles was detected by immunofluorescence microscopy in cultured A2780 cells. Cells were grown in microscopy slide chambers, exposed to **30** (5 or 50 nM) or vehicle (0.1% DMSO final concentration) for 16 h, and then permeabilized and fixed with 100 mM Pipes buffer (pH 6.8) containing 10 mM EGTA, 1 mM MgCl₂, 0.2% Triton X-100, and 4% formaldehyde, for 10 min at room temperature (RT). The fixed cells were treated with 2% bovine serum albumin (BSA) in TBST (Tris-buffered saline containing 0.1% Tween-20) for 1 h to block nonspecific antibody binding. Subsequently, cells were incubated with an anti- α -tubulin monoclonal antibody (clone DM1, Sigma) (1:500) for 12 h at 4 °C, followed by an incubation with a FITC-conjugated donkey antimouse IgG (15 μ g/mL) for 1 h at RT in the dark. Cells were then treated with the DNA stain Hoechst 33342 (10 μ g/mL) for 10 min, and slides were mounted with an antifade kit. Between staining steps, cells were washed 3 times with TBST. Mitotic spindles were visualized by a fluorescence microscope.

Caspase-3 Assay. A2780 cells were seeded at 20 000 cells/well in 96-well plates and grown overnight. Cells were treated in triplicate with vehicle (DMSO) or **30** for 48 h. The final concentration of compound in the assay ranged from 300 to 0.415 nM in a 7-point, 3-fold dilution series, and the final DMSO concentration was 0.1% v/v. Cells were lysed and the caspase-3 activity in cell lysates was determined using the ApoAlert caspase fluorescent assay kit according to the manufacturer's protocol. For compound **30**, EC₅₀ = 2.7 \pm 0.4 nM (n = 6).

hERG Binding Assay. The binding assay was performed on membrane preparations from human embryonic kidney (HEK) cells constitutively expressing hERG. The membranes were prepared by homogenization of the HEK cells in Tris-EDTA buffer (50 mM Tris, 1 mM EDTA, pH 7.5) and centrifugation at 45000g for 20 min at 4 °C. The pellet containing membrane was resuspended in Tris-EDTA and stored at -70 °C. In the binding assay, hERG membranes were diluted into assay buffer (60 mM KCl, 71.5 mM NaCl, 1 mM CaCl₂, 10 mM Hepes, pH 7.4) to a final concentration of 4.16 μ g per 400 μ L well volume. Radiolabeled ligand (³⁵S-MK-499, specific activity of ~1000 Ci/mmol) was then added to a final concentration of 50 pM, and 400 μ L of membrane-ligand mixture was added per well to 96-well assay blocks containing 4 μ L of 100 \times stocks of tested drugs or 100% DMSO (maximum binding control) or 100 μ M cold MK-499 (nonspecific binding control). Membranes were incubated at room temperature for 75 min, filtered through GF/B Unifilters presoaked in 0.1% BSA, and washed 5 \times 500 μ L with wash buffer at 4 °C (10 mM Hepes, 131.5 mM NaCl, 1 mM CaCl₂, 2 mM MgCl₂, pH 7.4). Filters were dried at room temperature, 50 μ L Microscint-20 was added to each well, and Unifilters were counted for 1 min. Dose-inhibition curves and inflection points were determined by curve-fitting the equation $\text{response} = ((\text{max} - \text{min}) / (1 + ([I]/IP)^s)) + \text{min}$, where I is the concentration of inhibitor, max is the maximum response (DMSO control), min is the minimum response (excess, cold ligand control), IP is the inflection point, and s is the slope. Generally, the inflection point is similar to the concentration of drug that inhibits 50% of radiotracer binding. Compounds were tested as an 8-point titration series, with 4-fold dilutions between each step, ranging from a concentration of 100 μ M (in assay) to 6 nM.

MDR Ratio. The human KB-3-1 tumor cell line and a multidrug-resistant derivative that overexpresses MDR1 (KB-V-1) were used to evaluate the MDR ratio. The KB-V-1 cell line was originally derived by culturing KB-3-1 cells in vinblastine and displays cross-resistance to multiple cancer drugs.³⁹ Relative to KB-3-1, KB-V-1 expresses >500-fold higher levels of MDR1 mRNA. Compounds

were evaluated for their ability to induce mitotic arrest in KB-3-1 and KB-V-1 cells by the phospho-nucleolin/mitotic arrest assay essentially as described above except that the final concentration of compound in the assay ranged from 10 000 to 0.1 nM in an 11-point, half-log dilution series. The MDR ratio is calculated by dividing the IC₅₀ in KB-V-1 cells by the IC₅₀ in KB-3-1 cells. Coadministration of verapamil, a competitive inhibitor of Pgp, restores the activity of paclitaxel and KSP inhibitors in the KB-V-1 cell line to nearly that observed in the parental KB-3-1 line, confirming that Pgp efflux is responsible for the observed resistance to drug-mediated mitotic arrest.

In Vivo Mitotic Arrest Assay. Subcutaneous (sc) xenograft tumors were formed by injection of the human A2780 ovarian carcinoma cell line in the hind flank of 8–12 week-old female immunodeficient nude mice (CrI:NU/NU-nuBR strain). Typically, animal weight ranged from 25 to 30 g. To facilitate tumor formation, cells were injected in media containing Matrigel, a solubilized basement membrane preparation extracted from the EHS mouse sarcoma. A2780 cells were grown in cell factories in RPMI medium + 10% serum, harvested by trypsinization and centrifugation, and resuspended in a 60:40 mixture of ice cold Matrigel/serum-free RPMI. Mice were lightly anesthetized via CO₂ inhalation, and 0.5 mL of cells (9 million) was injected sc into their hind flanks. On day 14 after tumor cell implantation, tumors were calipered and mice whose tumor volumes ranged typically from 300–900 mm³ were selected for study. Mice were randomized according to tumor volumes and distributed into treatment groups of 6 mice with approximately equivalent ranges of tumor volumes between treatment groups. On day 15 after tumor implantation, mice were implanted with Alzet 2001D osmotic pumps containing vehicle, positive control (compound **19** from ref 13b), or varying concentrations of **30** solubilized in water acidified to pH 4.0 with HCl. The dose groups (7 mice per group) of **30** were 40 (mg/kg)/day (5.78 mg/mL), 20 (mg/kg)/day (2.89 mg/mL), 10 (mg/kg)/day (1.45 mg/mL), 5 (mg/kg)/day (0.72 mg/mL), and 2.5 (mg/kg)/day (0.36 mg/mL). Pumps were primed for 3 h at 37 °C in 0.9% saline bath prior to implantation. For pump implantation, mice were anesthetized by intraperitoneal (ip) injection of ~0.1 mL of 7.7 mg/mL ketamine/0.46 mg/mL xylazine/0.9% saline mixture per 10 g body weight (typically, ~25–28 g). Implantation involved cranial-caudal incision on the right dorso-lateral flank, and incisions were sutured with surgical staples. Mice were euthanized 22 h after pump implantation by CO₂ inhalation, tumors were excised for PD analysis (see below for method), and blood was removed by cardiac puncture using heparinized 20-gauge needles. Plasma was prepared from heparinized whole blood by centrifugation at 3000 rpm for 15 min at 4 °C and stored frozen prior to analysis for levels of **30**. Tumors were excised during necropsy and fixed for 24–48 h in 10% formalin (saline buffered). Tissues were paraffin-embedded, thin-sectioned (5 μ m), and subject to antigen retrieval by heating (8 min, 20% microwave power) in target retrieval solution. Sections were immunostained with 1:200 diluted rabbit polyclonal anti-phosphohistone H3-Ser10 antibody followed by incubation with biotinylated goat antirabbit IgG [H + L] and then avidin-HRP. Signal was detected by development with HistoMark Black HRP substrate, followed by counterstaining with light-green counterstain. Immunostained tumor sections were quantitated by automated image acquisition and analysis. Images were captured using an inverted microscope fitted with a motorized stage and a digital camera. The percent of tumor area positively immunostained with phosphohistone H3-Ser10 was quantitated from the acquired images using Image Pro Plus software equipped with a custom macro. Necrotic regions of the tumor and regions with sporadic cellularity consisting primarily of Matrigel were excluded from the analysis. To eliminate subjectivity, data analysis using the Image Pro software was performed in a blinded fashion by two scientists. For each analyst's data set, percent phosphohistone H3 stained tumor area in each drug treated tumor was normalized to the mean percent phosphohistone H3 stained tumor area in the vehicle control group to determine the fold induction in mitotic arrest (phosphohistone H3 staining) for each drug treated tumor. Fold-induction values for

each tumor from the two analysts were averaged, and the mean \pm SEM for each drug treatment group was calculated. The minimum plasma concentration required to induce the maximum amount of mitotic arrest in the tumor is defined as the EC₉₀ for in vivo activity.

Tumor Growth Inhibition Assay. The mice for the dual flank xenograft were generated as described above for nude mouse xenograft formation but were raised by subcutaneous injection of either 9 million A2780 and 6 million PTX10 cells (method A) or 2.5 million KB-3-1 and 9 million KB-v-1 cells (method B) on contralateral flanks. On day 13–14 after tumor cell implantation, tumors were calipered and mice whose tumor volumes ranged typically from 250 to 500 mm³ were selected. Mice were randomized and distributed into treatment groups with approximately equivalent ranges of tumor volumes. For sc injection, **30** was formulated as a solution in acidified saline at pH 4.0, 100 μ L was administered for a dose of 100 mpk on the q4d \times 3 schedule (A2780/PTX10 experiment) or as a suspension in 0.5% w/v methylcellulose, and 100 μ L was administered for a dose of 40 mpk on the qd \times 1 schedule (KB-3-1/KB-v experiment). Paclitaxel was solubilized in a 1:1 (v/v) mixture of ethanol and Cremaphor-EL and then diluted in saline just prior to injection to make a working stock solution with final vehicle composition being ethanol/cremaphor/saline (10:10:80). Then 200 μ L of this working solution was injected ip in mice daily for 5 consecutive days (qd \times 5), delivering a dose of 20 mg/kg per day.

For efficacy evaluation, groups of 10–12 mice were dosed as indicated and their tumors were manually calipered on multiple days over the course of the study. Tumor volumes were evaluated for at least 10–11 days from the start of dosing. Tumor volumes were calculated according to the formula for volume of a prolate ellipsoid, $(W^2 \times L)/2$, where W (width) and L (length) are in millimeters and $L \geq W$. The mean tumor volume change ΔV , for treatment (T) and control (C) groups was calculated by subtracting the initial tumor volume (T_i), obtained either the day prior to start of treatment ($d - 1$) or on the same day as the start of treatment but prior to administration of compound, from the tumor volume on the day of testing, 3–14 days after start of dosing. Percent change in tumor volume in the treatment group relative to control group (% T/C) was calculated as follows:

$$\% (T/C) = 100 \times (\Delta VT) / (\Delta VC) \quad \text{if } \Delta VT > 0$$

$$\% (T/C) = 100 \times (\Delta VT) / T_i \quad \text{if } \Delta VT < 0$$

The error for each data point was determined by the following equation, where StdDev is the standard deviation and n is the number of animals in the given treatment group:

$$\text{error} = \text{StdDev} / \sqrt{n}$$

(B) Chemistry. All solvents used were commercially available “anhydrous” grade, and reagents were utilized without purification unless otherwise noted. Nonaqueous reactions were carried out in oven- or heat-gun-dried glassware under a nitrogen atmosphere. Magnetic stirring was used to agitate the reactions, and they were monitored for completion by either TLC (silica gel 60, Merck KGaA) or LC/MS (Waters 2690 separations module with a YMC Pro 50 mm \times 3 mm i.d. C-18 column interfaced with a Waters Micromass ZMD spectrometer) utilizing a gradient of 0.05% TFA in water/acetonitrile with detection at 215 or 254 nm. A Smith-Creator microwave from Personal Chemistry was used for microwave heating, and a CombiFlash system utilizing RediSep cartridges by Teledyne Isco was utilized for silica gel chromatography with fraction collection at 254 nm. Reverse phase HPLC purification was carried out on a Waters HPLC (XBridge Prep C-18 5 μ M 19 mm \times 150 mm column) utilizing a gradient of 0.1% TFA in water/acetonitrile with sample collection triggered by photodiode array detection. The reported yields are for isolated pure compounds unless otherwise noted and were not extensively optimized. Analytical HPLC was carried out on the above-mentioned LCMS system with a nine minute gradient (method A) and on a Hewlett-Packard 1100 series HPLC with a Sunfire C-18 5 μ M 4.5 mm \times 50 mm column and a gradient of 0.1% H₃PO₄ in water/acetonitrile

(method B). Both methods provided purities as measured by UV detection at 215 nm. Proton NMR spectra were recorded on a Varian INOVA 500 MHz spectrometer, and all chemical shifts are referenced to an internal standard of tetramethylsilane. High resolving power accurate mass measurement electrospray (ES) and atmospheric pressure chemical ionization (APCI) mass spectral data were acquired by use of a Bruker Daltonics 7T Fourier transform ion cyclotron resonance mass spectrometer (FT-ICR MS). Optical rotations were determined at 23 °C on a Perkin-Elmer 241 spectrometer in the solvents and concentrations specified.

Methyl 4-Methylene-2-phenylpyrrolidine-2-carboxylate (4). To a suspension of phenylglycine methyl ester hydrochloride (1.0 kg, 4.96 mol), anhydrous Na₂SO₄ (1.2 kg, 8.5 mol), and benzaldehyde (520 g, 4.91 mol) in 7.0 L of CH₂Cl₂ in a 20 L jacketed reactor was added triethylamine (518 g, 5.13 mol). After the mixture was stirred for 6 days, the solids were filtered off and rinsed with an additional 4.7 L of CH₂Cl₂. The filtrates were combined and used as is for the following reaction. To the solution of crude imine in a total of 11.7 L of CH₂Cl₂ was added tetrabutylammonium hydrogen sulfate (178 g, 0.52 mol, and methallyl dichloride (2.0 kg, 16 mol). Rapid stirring was initiated, and 7.8 L of a 10 M NaOH solution was added. After the mixture was stirred at room temperature overnight, the layers were split, and the bottom aqueous layer was removed. To the reactor was added 6 L of 1 M HCl, stirring was carried out for 2 h, the layers were separated, and the aqueous layer was basified to pH 8 with Na₂CO₃ and extracted three times with EtOAc. The combined EtOAc extracts were concentrated to dryness, dissolved in CH₂Cl₂, washed with saturated aqueous NaHCO₃ and water, dried over Na₂SO₄, and concentrated to provide 375 g of crude **4** that was carried into the next step without further purification.

6-Methylene-7a-phenyltetrahydro-1H-pyrrolo[1,2-c][1,3]oxazol-3-one (5). A 20 L reactor was charged with 6.8 L of 1 M LAH in THF (6.8 mol) and cooled to 0 °C. A solution of crude **4** (375 g, 1.73 mol) in 2.0 L of THF was added to the reactor over 40 min, cooling was removed, and stirring was maintained for 1 h at room temperature. The reaction was carefully quenched with 257 mL water, followed by 257 mL of 15% NaOH, and then 770 mL of water. To the reactor was added 1.2 kg of Na₂SO₄. Stirring was maintained overnight, and the solids were filtered and washed with THF. The combined filtrates were concentrated to provide 320 g of a crude oil that was used in the next step without purification. This material was dissolved in 12 L of CH₂Cl₂, and to the mixture was added triethylamine (350 mL, 2.5 mol) and 1,1'-carbonyldiimidazole (357 g, 2.2 mol). After the mixture was stirred overnight at room temperature, the reaction was quenched with 1 M HCl, the layers were split, and the organic was washed with water. The organic phase was dried over Na₂SO₄ and concentrated to provide 336 g of **5** as a crude oil that was used in the next step without purification.

7a-Phenyldihydro-1H-pyrrolo[1,2-c][1,3]oxazole-3,6(5H)-dione (6). Crude **5** (336 g, 1.56 mol) was dissolved in CH₂Cl₂ and split into two equal portions to process separately. The solution was cooled to -78 °C and purged with O₂, and then ozone was bubbled through the solution at a rate of 5 L/min until a pale-blue color persisted (~4 h). The mixture was purged of excess ozone, quenched dropwise with excess dimethyl sulfide (500 mL, ~10 equiv), and allowed to slowly warm to room temperature overnight with stirring. The two runs were pooled, the solvents were removed by rotary evaporation, and the solid was triturated with acetone to provide 160 g of **6** (15% from phenylglycine methyl ester) as a white solid. ¹H NMR (500 MHz, DMSO-*d*₆) δ 7.4 (m, 4H), 7.35 (m, 1H), 4.85 (d, J = 8.9 Hz, 1H), 4.30 (d, J = 8.9 Hz, 1H), 4.0 (d, J = 18.3 Hz, 1H), 3.55 (d, J = 18.3 Hz, 1H), 3.35 (d, J = 17.4 Hz), 2.90 (d, J = 17.4 Hz, 1H) ppm. LC/MS: t_R = 2.35 min (98% pure). LRMS = 218.0 (M + H).

6-(2,5-Difluorophenyl)-7a-phenyl-5,7a-dihydro-1H-pyrrolo[1,2-c][1,3]oxazol-3-one (7). A suspension of **6** (12.5 g, 57.5 mmol) in 500 mL of THF was cooled to -78 °C. With rapid stirring, a 1 M solution of NaHMDS (69 mL, 69 mmol) was added dropwise and allowed to age for 30 min before warming to 0 °C for 1 h. The

solution was cooled back to $-78\text{ }^{\circ}\text{C}$, and solid *N*-phenylbis(trifluoromethanesulfonylimide) (24.7 g, 69 mmol) was added in one portion. The mixture was allowed to warm slowly to room temperature overnight and quenched with a saturated solution of NH_4Cl . The organic layer was separated, and the aqueous phase was extracted twice with EtOAc. The combined organic phases were washed with brine, dried over Na_2SO_4 , and concentrated. This residue was dissolved in 400 mL of 1,2-dimethoxyethane, and to this was added 100 mL of water, LiCl (7.3 g, 172 mmol), Na_2CO_3 (18.3 g, 172 mmol), and 2,5-difluorophenylboronic acid (16 g, 101 mmol). The solution was degassed with N_2 for 2 min, charged with tetrakis(triphenylphosphine)palladium(0) (3.5 g, 3 mmol), and heated to $90\text{ }^{\circ}\text{C}$ for 3 h. After the mixture was cooled to room temperature, most of the DME was removed by distillation and the crude reaction was dumped into a separatory funnel with 500 mL of CH_2Cl_2 and 200 mL of water. The layers were cut, and the aqueous layer was extracted twice more with CH_2Cl_2 . The combined organic phase was washed with water, dried over Na_2SO_4 , and concentrated by rotary evaporation. The residue was dry loaded on silica and purified by column chromatography with a gradient of 0–100% CH_2Cl_2 in hexanes to provide semipure **7** as a white solid. This material was triturated with 150 mL of Et_2O , stirred overnight, and filtered to provide 12.5 g (69%) of **7** as a white solid. $^1\text{H NMR}$ (500 MHz, CDCl_3) δ 7.4 (m, 4H), 7.35 (m, 1H), 7.05 (m, 1H), 6.95 (m, 2H), 6.80 (d, $J = 1.0\text{ Hz}$, 1H), 4.85 (d, $J = 15.0\text{ Hz}$, 1H), 4.75 (d, $J = 8.7\text{ Hz}$, 1H), 4.50 (d, $J = 8.7\text{ Hz}$, 1H), 4.20 (m, 1H) ppm. LC/MS: $t_{\text{R}} = 4.56\text{ min}$ (96% pure). LRMS = 313.9 (M + H).

4-(2,5-Difluorophenyl)-2-phenyl-2-[(1,1,2,2-tetramethylpropoxy)methyl]-2,5-dihydro-1H-pyrrole (8). To a suspension of **7** (12.2 g, 38.9 mmol) in 120 mL of EtOH was added 3 M NaOH (77.9 mL, 233 mmol). The mixture was heated to $60\text{ }^{\circ}\text{C}$ for 4 h, cooled to room temperature, and added to a separatory funnel containing 250 mL of CHCl_3 and saturated brine. The layers were separated, and the aqueous phase was extracted twice with 2:1 $\text{CHCl}_3/\text{EtOH}$. The combined organic layers were washed with brine and concentrated. This residue was suspended in 100 mL of CH_2Cl_2 and 40 mL of DMF. Imidazole (10.6 g, 156 mmol) and TBSCl (12.3 g, 82 mmol) were added. The mixture was allowed to stir overnight, and it was added to a separatory funnel containing water and CH_2Cl_2 . The organic phase was washed several times with water, dried over Na_2SO_4 , and concentrated to an amber oil. This crude material was dissolved in 100 mL of MeOH and treated with $\sim 100\text{ mL}$ of 2 M methylamine in MeOH for 4 h at room temperature (to cleave the *N*-TBS group on the core). Following concentration by rotary evaporation, the residue was purified by column chromatography with a gradient of 0–40% EtOAc in hexanes to provide 12.9 g (83%) of **8** as a white solid. LC/MS: $t_{\text{R}} = 4.03\text{ min}$ (100% pure). LRMS = 402.0 (M + H).

(2S)-4-(2,5-Difluorophenyl)-2-phenyl-2-[(1,1,2,2-tetramethylpropoxy)methyl]-2,5-dihydro-1H-pyrrole [(S)-8]. Resolution of the enantiomers of **8** was carried out chromatographically using a Chiralpak AD 10 cm \times 50 cm column with 1% isopropanol in hexanes (containing 0.1% diethylamine as a modifier) at 175 mL/min. Injection of 20 g per run was determined to be optimal, with retention times of 35–55 min for peak 1 and 60–95 min for peak 2 and recovery of $>95\%$. Analytical HPLC analysis of the eluent, carried out on a 4 mm \times 250 mm Chiralpak AD column with the same eluent as above at a flow rate of 1 mL/min, indicated that the first enantiomer to elute ($t_{\text{R}} = 7.97\text{ min}$) was $>99\%$ ee and the second peak to elute ($t_{\text{R}} = 10.0\text{ min}$) was $\sim 99\%$ ee. The first enantiomer to elute is the desired (*S*)-isomer as determined by KSP activity and X-ray analysis of subsequent analogues (see US2005/0038074 for small-molecule X-ray analysis of **30**). Data for (*S*)-**8**: $^1\text{H NMR}$ (500 MHz, CDCl_3) δ 7.55 (m, 2H), 7.37 (m, 2H), 7.28 (m, 1H), 7.05 (m, 1H), 6.95 (m, 2H), 6.75 (d, $J = 1.6\text{ Hz}$, 1H), 4.42 (d, $J = 14.0\text{ Hz}$, 1H), 4.10 (dd, $J = 14.0, 1.6\text{ Hz}$, 1H), 3.94 (d, $J = 10.2\text{ Hz}$, 1H), 3.74 (d, $J = 10.2\text{ Hz}$, 1H), 2.57 (bs, 1H), 0.85 (s, 9H), 0.02 (s, 3H), 0.00 (s, 3H) ppm. LC/MS: $t_{\text{R}} = 4.03\text{ min}$ (100% pure). LRMS = 402.0 (M + H). $[\alpha]_{\text{D}} +28.4$ (c 1.0, chloroform).

(2S)-4-(2,5-Difluorophenyl)-2-(hydroxymethyl)-*N,N*-dimethyl-2-phenyl-2,5-dihydro-1H-pyrrole-1-carboxamide (9). To a suspension of triphosgene (3.7 g, 12.5 mmol) in 400 mL of THF at $0\text{ }^{\circ}\text{C}$ was added a solution of (*S*)-**8** (10 g, 24.9 mmol) and triethylamine (5.2 mL, 37.4 mmol) in THF over $\sim 2\text{ min}$. After the mixture was warmed and stirred for 1 h at room temperature, a 2 M solution of dimethylamine in THF (50 mL, 100 mmol) was added and stirring was continued for 2 h. The mixture was added to a separatory funnel containing 100 mL of 1 M HCl, and the mixture was extracted twice with EtOAc. The combined organic layers were washed again with HCl and then with brine, dried over Na_2SO_4 , and concentrated. The residue was dissolved in 300 mL of THF and cooled to $0\text{ }^{\circ}\text{C}$, and 4 M HCl in dioxane (25 mL, 100 mmol) was added dropwise. The mixture was allowed to warm to room temperature and was stirred for 2 h before being added to a separatory funnel containing 5% aqueous Na_2CO_3 . The mixture was extracted twice with EtOAc, washed with saturated brine, dried over Na_2SO_4 , and concentrated. The residue was purified by column chromatography with a gradient of 2–100% EtOAc in hexanes to provide 7.0 g (78%) of **9** as a white solid. $^1\text{H NMR}$ (500 MHz, CDCl_3) δ 7.35 (m, 4H), 7.25 (m, 1H), 7.05 (m, 1H), 6.95 (m, 2H), 6.28 (s, 1H), 5.46 (m, 1H), 4.86 (d, $J = 13.8\text{ Hz}$, 1H), 4.63 (d, $J = 13.8\text{ Hz}$, 1H), 4.42 (m, 1H), 4.00 (d, $J = 12.2\text{ Hz}$, 1H), 2.98 (s, 6H) ppm. HPLC purity: method A = 100%; method B = 98.5%. HRMS calcd for $\text{C}_{20}\text{H}_{20}\text{F}_2\text{N}_2\text{O}_2$ (M + H): 359.1566. Found: 359.1564. $[\alpha]_{\text{D}} -66.4$ (c 1.0, chloroform).

(2S)-4-(2,5-Difluorophenyl)-2-(hydroxymethyl)-*N*-methyl-*N*-(1-methylpiperidin-4-yl)-2-phenyl-2,5-dihydro-1H-pyrrole-1-carboxamide (11). To a suspension of triphosgene (982 mg, 9.7 mmol) in 100 mL of THF at $0\text{ }^{\circ}\text{C}$ was added a solution of (*S*)-**8** (2.6 g, 6.5 mmol) and triethylamine (1.35 mL, 9.7 mmol) in THF over $\sim 2\text{ min}$. After stirring for 1 h at $0\text{ }^{\circ}\text{C}$, the mixture was warmed to room temperature and stirred for an additional 2 h. The reaction was quenched with saturated aqueous brine, added to a separatory funnel containing EtOAc, and the layers were cut. The aqueous phase was extracted again with EtOAc and the combined organic layers were washed with saturated brine, dried over Na_2SO_4 , and concentrated to provide the intermediate carbamoyl chloride. This material was dissolved in 100 mL of CH_2Cl_2 , and 4-methylamino-*N*-methylpiperidine (1.67 g, 13 mmol) and triethylamine (2.7 mL, 19.4 mmol) were added, followed by a catalytic amount of DMAP. After being stirred overnight at room temperature, the mixture was added to a separatory funnel containing saturated aqueous NaHCO_3 , and the mixture was extracted twice with CH_2Cl_2 . The combined organic layers were washed with water, dried over Na_2SO_4 , and concentrated. The residue was purified by column chromatography with a gradient of 0–50% 20:1:1 EtOH/ H_2O / NH_4OH in EtOAc to provide a colorless oil. This residue was dissolved in 150 mL of THF. The mixture was cooled to $0\text{ }^{\circ}\text{C}$, and 4 M HCl in dioxane (6.5 mL, 26 mmol) was added dropwise. The mixture was allowed to warm to room temperature and was stirred for 2 h before being added to a separatory funnel containing 5% aqueous Na_2CO_3 . The mixture was extracted twice with EtOAc, washed with saturated brine, dried over Na_2SO_4 , and concentrated. An attempt to purify the residue by column chromatography with a gradient of 0–50% 20:1:1 EtOH/ H_2O / NH_4OH in EtOAc provided $\sim 2\text{ g}$ of **11** (70%) as a white solid but with only 87% purity. Analytically pure material was obtained by reverse phase HPLC purification of a portion of this material and free-basing the fractions with NaHCO_3 . The basic fractions were extracted with EtOAc, dried over Na_2SO_4 , and concentrated to provide 380 mg of **11** as a white solid. $^1\text{H NMR}$ (500 MHz, CDCl_3) δ 7.35 (m, 4H), 7.25 (m, 1H), 7.05 (m, 1H), 6.95 (m, 2H), 6.29 (s, 1H), 5.40 (m, 1H), 4.83 (d, $J = 13.7\text{ Hz}$, 1H), 4.57 (d, $J = 13.7\text{ Hz}$, 1H), 4.42 (m, 1H), 4.00 (d, $J = 12.0\text{ Hz}$, 1H), 3.71 (m, 1H), 2.95 (m, 2H), 2.90 (s, 3H), 2.29 (s, 3H), 2.10 (m, 2H), 2.0–1.8 (m, 3H), 1.65 (m, 1H) ppm. HPLC purity: method A = 100%; method B = 100%. HRMS calcd for $\text{C}_{25}\text{H}_{29}\text{F}_2\text{N}_3\text{O}_2$ (M + H): 442.2301. Found: 442.2300. $[\alpha]_{\text{D}} -41.9$ (c 1.0, chloroform).

Benzyl 3-Fluoro-4-oxopiperidine-1-carboxylate (18). To a solution of benzyl-4-oxo-1-piperidinecarboxylate (50 g, 215 mmol) in 225 mL of DMF was added triethylamine (90 mL, 644 mmol) and then chlorotrimethylsilane (38.1 mL, 300 mmol). The mixture

was heated at 80 °C overnight, cooled to room temperature, and then dumped into a separatory funnel containing hexanes. The mixture was partitioned with water, washed with brine, dried over Na₂SO₄, and concentrated by rotary evaporation. The residue was dissolved in 1000 mL of CH₃CN, cooled to 0 °C, and treated with Selectfluor (79.8 g, 225 mmol) in three portions over 5 min. After the mixture was stirred at room temperature overnight, most of the solvent was removed by rotary evaporation and then partitioned between EtOAc and water, separated, washed with saturated brine solution, dried over MgSO₄, filtered, and concentrated by rotary evaporation. The residue was purified by column chromatography with a gradient of 33–66% EtOAc in hexanes to provide 48.5 g (90%) of **18** as a white solid. LRMS = 252 (M + H).

(±)-*trans*-Benzyl 3-Fluoro-4-(methylamino)piperidine-1-carboxylate (**19**) and (±)-*cis*-Benzyl 3-Fluoro-4-(methylamino)piperidine-1-carboxylate (**20**). To a solution of **18** (10 g, 39.8 mmol) in 100 mL of MeOH was added acetic acid (~5 mL) and a 2 M solution of methylamine in THF (60 mL, 120 mmol). After the mixture was stirred for 3 h, NaCNBH₃ (3.76 g, 60 mmol) was added. After the mixture was stirred overnight, the reaction was quenched with saturated aqueous NaHCO₃, partitioned with CH₂Cl₂, washed with brine, dried over MgSO₄, filtered, and concentrated by rotary evaporation. The residue was loaded onto a silica gel column and eluted with EtOAc, then 80:10:10 CHCl₃/EtOAc/MeOH to provide 3.7 g (35%) of **19** (100% pure) and 2.9 g (27%) of **20** (100% pure) as colorless oils. Data for **19**, first to elute (confirmed by NOE analysis at -35 °C): ¹H NMR (500 MHz, CD₂Cl₂) δ 7.4–7.3 (m, 5H), 5.1 (m, 2H), 4.4–4.1 (m, 2H), 3.9 (m, 1H), 3.15–3.05 (m, 2H), 2.75 (m, 1H), 2.4 (s, 3H), 2.0 (m, 1H), 1.25 (m, 1H) ppm. Data for **20**, second to elute (confirmed by NOE analysis at -35 °C): ¹H NMR (500 MHz, CD₂Cl₂) δ 7.4–7.2 (m, 5H), 5.1 (m, 2H), 4.9–4.7 (m, 1H), 4.4 (m, 1H), 4.15 (m, 1H), 3.1–2.9 (m, 2H), 2.6 (m, 1H), 2.4 (s, 3H), 1.8 (m, 1H), 1.6 (m, 1H) ppm. HRMS calcd for C₂₆H₃₀F₃N₃O₂ (M + H): 267.1504. Found: 267.1500. By a change of solvents, the *cis*-isomer can be obtained as the major product: To a solution of **18** (50.5 g, 201 mmol) in 700 mL of 1,2-dichloroethane was added a 2 M solution of methylamine in THF (201 mL, 402 mmol). After the mixture was stirred for 2 h, Na(OAc)₃BH (64 g, 302 mmol) was added. After the mixture was stirred overnight, the reaction was quenched with saturated aqueous K₂CO₃, partitioned with CH₂Cl₂, separated, and the aqueous phase was extracted three times with CH₂Cl₂. The combined organic extracts were washed with brine, dried over MgSO₄, filtered, and concentrated by rotary evaporation. The residue was loaded onto a silica gel column and eluted with EtOAc, then 90:5:5 CHCl₃/EtOAc/MeOH, and finally 80:10:10 CHCl₃/EtOAc/MeOH. The column was repeated twice more on mixed fractions to provide 7 g (13%) of **19** and 38.7 g (72%) of **20** (100% pure).

Benzyl (3*S*,4*R*)-4-[(*tert*-Butoxycarbonyl)(methyl)amino]-3-fluoropiperidine-1-carboxylate (**23**) and Benzyl (3*R*,4*S*)-4-[(*tert*-Butoxycarbonyl)(methyl)amino]-3-fluoropiperidine-1-carboxylate (**24**). To a solution of **20** (2.9 g, 10.9 mmol) in 55 mL of CH₂Cl₂ was added triethylamine (4.6 mL, 30.3 mmol) and di-*tert*-butyl dicarbonate (3.6 g, 16.4 mmol). After being stirred for 48 h, the mixture was partitioned between CH₂Cl₂ and H₂O, and the organic phase was washed with brine, dried over MgSO₄, filtered, and concentrated by rotary evaporation. The residue was loaded onto a silica gel column in CHCl₃ and eluted with a gradient of 0–33% EtOAc in hexanes to provide a white solid. Resolution of the enantiomers was carried out chromatographically using a Chiralpak AD 10 cm × 50 cm column with 20% isopropanol in hexanes (with 0.1% diethylamine) at 150 mL/min to provide 1.78 g (45%) of the first eluting enantiomer **23** and 1.64 g (41%) of the second eluting enantiomer **24** (the absolute stereochemistry of **24** is assigned by small-molecule X-ray analysis of subsequent analogues (see US2005/0038074 or WO2005/102996). Analytical HPLC analysis of the eluent on a 4 mm × 250 mm Chiralpak AD column with 20% isopropanol in hexanes (with 0.1% diethylamine) at 1 mL/min indicated that **23** has *t*_R = 5.69 min and >98% ee and **24** has *t*_R = 6.52 min and ee = 98%. Data for **24**: ¹H NMR (500 MHz, CDCl₃, extensive broadening at 25 °C) δ 7.4–7.3 (m, 5H),

5.13 (bs, 2H), 4.9–4.6 (m, 1H), 4.6–3.9 (m, 3H), 3.1–2.9 (m, 2H), 2.85 (bs, 3H), 2.15 (m, 1H), 1.5 (m, 1H), 1.47 (bs, 9H) ppm. HPLC purity: method A = 100%; method B = 100%. HRMS calcd for C₁₉H₂₇FN₂O₄ (M + Na): 389.1847. Found: 389.1847. [α]_D²⁰ -72.9 (c 1.0, chloroform).

(3*R*,4*S*)-3-Fluoro-*N*,1-dimethylpiperidin-4-amine (**28**). To a solution of **24** (4.6 g, 12.5 mmol) in 150 mL of EtOH was added 1,4-cyclohexadiene (29.9 mL, 313 mmol) and 10% Pd on carbon (~1 g). After being stirred overnight, the mixture was filtered through Celite and concentrated by rotary evaporation. The residue was dissolved in 75 mL of MeOH. Acetic acid (~2 mL) and 37% aqueous formaldehyde (30.1 mL, 38 mmol) were added, and the mixture was stirred for 1 h. At that time, NaCNBH₃ (1.58 g, 25.1 mmol) in 10 mL of MeOH was added and the mixture was aged for 2 h before being dumped into saturated aqueous NaHCO₃. After extracting three times with CH₂Cl₂, the organic phase was washed with water, dried over MgSO₄, filtered, and concentrated by rotary evaporation to provide 3.0 g of a colorless oil. LRMS = 247.2 (M + H). A portion of this material (1.43 g, 5.8 mmol) in 50 mL of EtOAc was treated with HCl gas until the solution was warm to the touch. The flask was capped and stirred for 2 h. The volatiles were removed by rotary evaporation, and the residue was triturated with Et₂O and placed under high vacuum to provide a white solid. This material was partitioned between 5% aqueous Na₂CO₃ and 2:1 CHCl₃/EtOH. The layers were cut, and the aqueous phase was extracted twice more with 2:1 CHCl₃/EtOH. The combined organic layers were washed with saturated brine and concentrated by rotary evaporation and the residue was dissolved in CH₂Cl₂, dried over Na₂SO₄, and concentrated to provide 628 mg (50%) of **28** a colorless oil. ¹H NMR (500 MHz, CDCl₃) δ 4.8 (d, *J* = 48.9 Hz, 1H), 3.15 (m, 1H), 2.85 (m, 1H), 2.5 (s, 3H), 2.45 (m, 1H), 2.3 (s, 3H), 2.2–2.0 (m, 2H), 1.9–1.7 (m, 2H) ppm. HRMS calcd for C₇H₁₅FN₂ (M + H): 147.1292. Found: 147.1300.

(2*S*)-2-([*tert*-Butyl(dimethyl)silyloxy]methyl)-4-(2,5-difluorophenyl)-2-phenyl-2,5-dihydro-1*H*-pyrrole-1-carbonyl Chloride (**29**). To a suspension of triphosgene (7.76 g, 26.2 mmol) in 600 mL of THF at 0 °C was added a solution of (*S*)-**8** (21 g, 52.3 mmol) and triethylamine (11 mL, 79 mmol) over ~3 min. After being stirred for 1 h at 0 °C, the mixture was warmed to room temperature and stirred for an additional 3 h. The reaction was quenched with 300 mL of water, added to a separatory funnel containing EtOAc, and the layers were cut. The aqueous phase was extracted again with EtOAc, and the combined organic layers were washed with saturated brine, dried over Na₂SO₄, concentrated, resuspended in CH₂Cl₂, and concentrated to provide **29** as a thick, colorless oil. This material is stable for months under nitrogen in a closed container at 0 °C. LC/MS (3.7 min run): *t*_R = 3.56 min (100% pure). LRMS = 464.1 (M + H).

(2*S*)-4-(2,5-Difluorophenyl)-*N*-[(3*R*,4*S*)-3-fluoro-1-methylpiperidin-4-yl]-2-(hydroxymethyl)-*N*-methyl-2-phenyl-2,5-dihydro-1*H*-pyrrole-1-carboxamide (**30**). To a solution of **29** (1.6 g, 3.45 mmol) in 25 mL of THF was added **28** (630 mg, 4.3 mmol), triethylamine (1.44 mL, 10.3 mmol), and a catalytic amount of DMAP. After being stirred for 24 h at room temperature, the mixture was partitioned between EtOAc and saturated aqueous NaHCO₃, and the organic layer was washed with brine, dried over Na₂SO₄, and concentrated by rotary evaporation. The residue was purified by silica gel chromatography with 0–10% MeOH in CH₂Cl₂ (containing ~0.5% triethylamine) to provide ~1.7 g of a pale-yellow taffy. This material was dissolved in 75 mL of CH₃CN, 3 mL of triethylamine trihydrofluoride was added, and the mixture was stirred for 24 h at room temperature. An additional 3 mL of triethylamine trihydrofluoride was added, and the mixture was heated at 37 °C for 24 h. The mixture was cooled to room temperature, dumped into saturated aqueous NaHCO₃, extracted three times with EtOAc, washed with brine, dried over Na₂SO₄, and concentrated by rotary evaporation. The residue was purified by silica gel chromatography with a gradient of 0–50% 20:1:1 EtOH/NH₄OH/H₂O in EtOAc to provide 1.0 g (63%) of **30** as a white solid. ¹H NMR (500 MHz, CDCl₃) δ 7.35 (m, 4H), 7.25 (m, 1H), 7.05 (m, 1H), 6.95 (m, 2H), 6.28 (s, 1H), 5.22 (dd, *J* = 8.8,

3.7 Hz, 1H), 4.92 (d, $J = 13.7$ Hz, 1H), 4.80 (d, $J = 50.3$ Hz, 1H), 4.62 (d, $J = 13.8$ Hz, 1H), 4.44 (m, 1H), 4.1–4.0 (m, 2H), 3.15 (m, 1H), 3.11 (s, 3H), 3.0 (m, 1H), 2.4–2.1 (m, 3H), 2.31 (s, 3H), 1.70 (m, 1H) ppm. HPLC purity: method A = 100%; method B = 100%. HRMS calcd for $C_{25}H_{28}F_3N_3O_2$ (M + H): 460.2206. Found: 460.2213. $[\alpha]_D -70.5$ (c 1.0, chloroform).

3-fluoropiperidine-1-carboxylate (21) and Benzyl (3R,4R)-4-[(tert-Butoxycarbonyl)(methylamino)-3-fluoropiperidine-1-carboxylate (22). To a solution of **19** (3.7 g, 13.9 mmol) in 70 mL of CH_2Cl_2 was added triethylamine (5.8 mL, 41.7 mmol) and di-*tert*-butyl dicarbonate (4.55 g, 20.9 mmol). After being stirred for 48 h, the mixture was partitioned between CH_2Cl_2 and H_2O , and the organic phase was washed with brine, dried over $MgSO_4$, filtered, and concentrated by rotary evaporation. The residue was loaded onto a silica gel column in $CHCl_3$ and eluted with a gradient of 0–33% EtOAc in hexanes to provide a white solid. Resolution of the enantiomers was carried out chromatographically using a Chiralpak AD 10 cm \times 50 cm column with 15% isopropanol in hexanes (with 0.1% diethylamine) at 150 mL/min to provide 2.3 g (45%) of the first eluting enantiomer **21** and 2.5 g (49%) of the second eluting enantiomer **22** (the absolute stereochemistry of **21** and **22** is not known but is tentatively assigned as shown to simplify visualization of the relative stereochemistry). Analytical HPLC analysis of the eluent on a 4 mm \times 250 mm Chiralpak AD column with 15% isopropanol in hexanes (with 0.1% diethylamine) at 1 mL/min indicated that **21** has $t_R = 7.41$ min and 98% ee and **22** has $t_R = 11.7$ min and ee = 98%. Data for **21**: 1H NMR (500 MHz, $CDCl_3$, extensive broadening at 25 °C) δ 7.4–7.3 (m, 5H), 5.12 (bs, 2H), 4.7–4.35 (m, 2H), 4.3–3.9 (m, 2H), 2.80 (bs, 5H), 1.8–1.6 (m, 2H), 1.46 (s, 9H) ppm. HPLC purity: method A = 100%; method B = 100%. HRMS calcd for $C_{19}H_{27}FN_2O_4$ (M + Na): 389.1847. Found: 389.1850. $[\alpha]_D -9.2$ (c 1.0, chloroform).

(2S)-4-(2,5-Difluorophenyl)-N-[(3S,4S)-3-fluoro-1-methylpiperidin-4-yl]-2-(hydroxymethyl)-N-methyl-2-phenyl-2,5-dihydro-1H-pyrrole-1-carboxamide (31). A procedure analogous to that used to prepare **30** was employed beginning with **21** to provide **31** as a white solid. 1H NMR (500 MHz, $CDCl_3$) δ 7.35 (m, 4H), 7.25 (m, 1H), 7.05 (m, 1H), 6.95 (m, 2H), 6.29 (s, 1H), 4.91 (bs, 1H), 4.85 (dd, $J = 14.2$, 1.5 Hz, 1H), 4.8–4.7 (m, 1H), 4.71 (d, $J = 12.8$ Hz, 1H), 4.45 (m, 1H), 4.03 (d, $J = 12.0$ Hz, 1H), 3.82 (m, 1H), 3.26 (m, 1H), 2.90 (s, 3H), 2.83 (m, 1H), 2.33 (s, 3H), 2.15 (m, 1H), 2.05–1.9 (m, 2H), 1.70 (m, 1H) ppm. HPLC purity: method A = 100%; method B = 100%. HRMS calcd for $C_{25}H_{28}F_3N_3O_2$ (M + H): 460.2206. Found: 460.2196. $[\alpha]_D -49.2$ (c 0.5, chloroform).

Acknowledgment. We thank Rick Woodward for the large-scale synthesis of intermediate **5**, Carl Homnick for determining chiral separation conditions for **8**, Dr. Chuck Ross and Joan Murphy for HRMS analysis, Dr. Steve Pitzenger for 2D and NOE NMR analyses, Matt Zrada for pK_a determinations, Dr. David Dubost for stability and solubility measurements, and Dr. Tito Fojo of the National Institutes of Health for access to the PTX10 cell line.

Supporting Information Available: Experimental procedures for compounds **12–16**, potency data for the epimers of **30** and **31**, and proton NMR spectra of all new compounds. This material is available free of charge via the Internet at <http://pubs.acs.org>.

References

- Chabner, B. A.; Roberts, T. G., Jr. Chemotherapy and the war on cancer. *Nat. Rev. Cancer* **2005**, *5*, 65–72.
- (a) Nadal, E.; Olavarria, E. Imatinib mesylate (Gleevec/Glivec) a molecular-targeted therapy for chronic myeloid leukaemia and other malignancies. *J. Clin. Pract.* **2004**, *58*, 511–516. (b) Hussain, S. A.; Palmer, D. H.; Spooner, D.; Rea, D. W. Molecularly targeted therapeutics for breast cancer. *BioDrugs* **2007**, *21*, 215–224. (c) Sun, S.; Schiller, J. H.; Spinola, M.; Minna, J. D. New molecularly targeted therapies for lung cancer. *J. Clin. Invest.* **2007**, *117*, 2740–2750. (d)

- Grandinetti, C. A.; Goldspiel, B. R. Sorafenib and sunitinib: novel targeted therapies for renal cell cancer. *Pharmacotherapy* **2007**, *27*, 1125–1144.
- Conlin, A. K.; Seidman, A. D. Taxanes in breast cancer: An update. *Curr. Oncol. Rep.* **2007**, *9*, 22–30.
- (a) Miglarese, M. R.; Carlson, R. O. Development of new cancer therapeutic agents targeting mitosis. *Expert Opin. Invest. Drugs* **2006**, *15*, 1411–1425. (b) Schmidt, M.; Bastians, H. Mitotic drug targets and the development of novel anti-mitotic anticancer drugs. *Drug Resist. Updates* **2007**, *10*, 162–181.
- Wood, K. W.; Cornwell, W. D.; Jackson, J. R. Past and future of the mitotic spindle as an oncology target. *Curr. Opin. Pharmacol.* **2001**, *1*, 370–377.
- Jackson, J. R.; Patrick, D. R.; Dar, M. M.; Huang, P. S. Targeted anti-mitotic therapies: can we improve on tubulin agents? *Nat. Rev. Cancer* **2007**, *7*, 107–117.
- (a) Goldstein, L. S. B.; Philp, A. V. The road less traveled: emerging principles of kinesin motor utilization. *Annu. Rev. Cell Dev. Biol.* **1999**, *15*, 141–183. (b) Mandelkow, E.; Mandelkow, E.-M. Kinesin motors and disease. *Trends Cell Biol.* **2002**, *12*, 585–591.
- (a) Sharp, D. J.; Rogers, G. C.; Scholey, J. M. Microtubule motors in mitosis. *Nature* **2000**, *407*, 41–47. (b) Heald, R. Motor function in the mitotic spindle. *Cell* **2000**, *102*, 399–402. (c) Bergnes, G.; Brejc, K.; Belmont, L. Mitotic kinesins: prospects for antimitotic drug discovery. *Curr. Top. Med. Chem.* **2005**, *5*, 127–145.
- (a) Mayer, T. U.; Kapoor, T. M.; Haggarty, S. J.; King, R. W.; Schreiber, S. L.; Mitchison, T. J. Small molecule inhibitor of mitotic spindle bipolarity identified in a phenotype-based screen. *Science* **1999**, *286*, 971–974. (b) Sakowicz, R.; Finer, J. T.; Beraud, C.; Crompton, A.; Lewis, E.; Fritsch, A.; Lee, Y.; Mak, J.; Moody, R.; Turincio, R.; Chabala, J. C.; Gonzales, P.; Roth, S.; Weitman, S.; Wood, K. W. Antitumor activity of a kinesin inhibitor. *Cancer Res.* **2004**, *64*, 3276–3280. (c) Jiang, C.; You, Q.; Li, Z.; Guo, Q. Kinesin spindle protein inhibitors as anticancer agents. *Expert Opin. Ther. Pat.* **2006**, *16*, 1517–1532.
- (a) Marcus, A. I.; Peters, U.; Thomas, S. L.; Garrett, S.; Zelnak, A.; Kapoor, T. M.; Giannakou, P. Mitotic kinesin inhibitors induce mitotic arrest and cell death in paclitaxel-resistant and -sensitive cancer cells. *J. Biol. Chem.* **2005**, *280*, 11569–11577. (b) Dutcher, J. P.; Novik, Y.; O'Boyle, K.; Marcoullis, G.; Secco, C.; Wiernik, P. H. 20th-Century advances in drug therapy in oncology. Part II. *J. Clin. Pharmacol.* **2000**, *40*, 1079–1092.
- Sorbera, L. A.; Bolos, J.; Serradell, N.; Bayés, M. Ispinesib mesilate. *Drugs Future* **2006**, *31*, 778–787.
- It is tempting to speculate that antimitotic agents designed to overcome known mechanisms of resistance, such as Pgp-overexpression and tubulin mutations, will lead to improved efficacy in the clinic against refractory tumors. Indeed, some recent studies have provided evidence in support of this hypothesis. See, for example, the following: (a) Toppmeyer, D.; Seidman, A. D.; Pollak, M.; Russell, C.; Tkaczuk, K.; Verma, S.; Overmoyer, B.; Garg, V.; Ette, E.; Harding, M. W.; Demetri, G. D. Safety and efficacy of the multidrug resistance inhibitor Incel (Biricodar; VX-710) in combination with paclitaxel for advanced breast cancer refractory to paclitaxel. *Clin. Cancer Res.* **2002**, *8*, 670–678. (b) Goodin, S.; Kane, M. P.; Rubin, E. H. Etoposides: mechanism of action and biologic activity. *J. Clin. Oncol.* **2004**, *22*, 2015–2025. However, results from these clinical trials, though positive, have been less than stellar, and the validity of this rationale is still often questioned. See the following: (c) Greenberger, L. M.; Sampath, D. Resistance to Taxanes. In *Cancer Drug Discovery and Development: Cancer Drug Resistance*; Teicher, B., Ed.; Humana Press Inc.: Totowa, NJ, 2006; pp 329–357. (d) Ferlini, C.; Raspaglio, G.; Cicchillitti, L.; Mozzetti, S.; Prislei, S.; Bartollino, S.; Scambia, G. Looking at drug resistance mechanisms for microtubule interacting drugs: Does TUBB3 work? *Curr. Cancer Drug Targets* **2007**, *7*, 704–712.
- (a) Cox, C. D.; Breslin, M. J.; Mariano, B. J.; Coleman, P. J.; Buser, C. A.; Walsh, E. S.; Hamilton, K.; Huber, H. E.; Kohl, N. E.; Torrent, M.; Yan, Y.; Kuo, L. C.; Hartman, G. D. Kinesin spindle protein (KSP) inhibitors. Part 1: The discovery of 3,5-dihydropyrazoles as potent and selective inhibitors of the mitotic kinesin KSP. *Bioorg. Med. Chem. Lett.* **2005**, *15*, 2041–2045. (b) Fraley, M. E.; Garbaccio, R. M.; Arrington, K. L.; Hoffman, W. F.; Tasber, E. S.; Coleman, P. J.; Buser, C. A.; Walsh, E. S.; Hamilton, K.; Fernandez, C.; Schaber, M. D.; Lobell, R. B.; Tao, W.; South, V. J.; Yan, Y.; Kuo, L. C.; Prueksaritanont, T.; Shu, C.; Torrent, M.; Heimbrosk, D. C.; Kohl, N. E.; Huber, H. E.; Hartman, G. D. Kinesin spindle protein (KSP) inhibitors. Part 2: The design, synthesis, and characterization of 2,4-diaryl-2,5-dihydropyrrole inhibitors of the mitotic kinesin KSP. *Bioorg. Med. Chem. Lett.* **2006**, *16*, 1775–1779. (c) Cox, C. D.; Torrent, M.; Breslin, M. J.; Mariano, B. J.; Whitman, D. B.; Coleman, P. J.; Buser, C. A.; Walsh, E. S.; Hamilton, K.; Schaber, M. D.; Lobell, R. B.; Tao, W.; South, V. J.; Kohl, N. E.; Yan, Y.; Kuo, L. C.; Prueksaritanont, T.; Slaughter, D. E.; Li, C.; Mahan, E.; Lu, B.; Hartman, G. D.

- Kinesin spindle protein (KSP) inhibitors. Part 4: Structure-based design of 5-alkylamino-3,5-diaryl-4,5-dihydropyrazoles as potent, water-soluble inhibitors of the mitotic kinesin KSP. *Bioorg. Med. Chem. Lett.* **2006**, *16*, 3175. (d) Cox, C. D.; Breslin, M. J.; Whitman, D. B.; Coleman, P. J.; Garbaccio, R. M.; Fraley, M. E.; Zrada, M. M.; Buser, C. A.; Walsh, E. S.; Hamilton, K.; Lobell, R. B.; Tao, W.; Abrams, M. T.; South, V. J.; Huber, H. E.; Kohl, N. E.; Hartman, G. D. Kinesin spindle protein (KSP) inhibitors. Part 5: Discovery of 2-propylamino-2,4-diaryl-2,5-dihydropyrazoles as potent, water-soluble KSP inhibitors, and modulation of their basicity by β -fluorination to overcome cellular efflux by P-glycoprotein. *Bioorg. Med. Chem. Lett.* **2007**, *17*, 2697–2702.
- (14) Coleman, P. J.; Schreier, J. D.; Cox, C. D.; Fraley, M. E.; Garbaccio, R. M.; Buser, C. A.; Walsh, E. S.; Hamilton, K.; Lobell, R. B.; Rickert, K.; Tao, W.; Diehl, R. E.; South, V. J.; Davide, J. P.; Kohl, N. E.; Yan, Y.; Kuo, L.; Prueksaritanont, T.; Li, C.; Mahan, E. A.; Fernandez-Metzler, C.; Salata, J. J.; Hartman, G. D. Kinesin spindle protein (KSP) inhibitors. Part 6: Design and synthesis of 3,5-diaryl-4,5-dihydropyrazole amides as potent inhibitors of the mitotic kinesin KSP. *Bioorg. Med. Chem. Lett.* **2007**, *17*, 5390–5395.
- (15) Roden, D. M. Drug-induced prolongation of the QT interval. *N. Engl. J. Med.* **2004**, *350*, 1013–1022.
- (16) Garbaccio, R. M.; Fraley, M. E.; Tasber, E. S.; Olson, C. M.; Hoffman, W. F.; Arrington, K. L.; Torrent, M.; Buser, C. A.; Walsh, E. S.; Hamilton, K.; Schaber, M. D.; Fernandez, C.; Lobell, R. B.; Tao, W.; South, V. J.; Yan, Y.; Kuo, L. C.; Prueksaritanont, T.; Slaughter, D. E.; Shu, C.; Heimbrook, D. C.; Kohl, N. E.; Huber, H. E.; Hartman, G. D. Kinesin spindle protein (KSP) inhibitors. Part 3: Synthesis and evaluation of phenolic 2,4-diaryl-2,5-dihydropyrazoles with reduced hERG binding and employment of a phosphate prodrug strategy for aqueous solubility. *Bioorg. Med. Chem. Lett.* **2006**, *16*, 1780–1783.
- (17) Jamieson, C.; Moir, E. M.; Rankovic, Z.; Wishart, G. Medicinal chemistry of hERG optimizations: highlights and hang-ups. *J. Med. Chem.* **2006**, *49*, 5029–5046.
- (18) By comparison, **2** had an MDR ratio of 4.6 with an EC_{50} of 26.4 nM in the overexpressing cell line.
- (19) For a review of the relevance of Pgp to drug discovery, see the following: Lin, J. H.; Yamazaki, M. Clinical relevance of P-glycoprotein in drug therapy. *Drug Metab. Rev.* **2003**, *35*, 417–454.
- (20) (a) Seelig, A. How does P-glycoprotein recognize its substrates? *Int. J. Clin. Pharmacol. Ther.* **1998**, *36*, 50–54. (b) Stouch, T. R.; Gudmundsson, O. Progress in understanding the structure–activity relationships of P-glycoprotein. *Adv. Drug Delivery Rev.* **2002**, *54*, 315–328.
- (21) Raub, T. J. P-Glycoprotein recognition of substrates and circumvention through rational drug design. *Mol. Pharm.* **2006**, *3*, 3–25.
- (22) Yates, C. R.; Chang, C.; Kearbey, J. D.; Yasuda, K.; Schuetz, E. G.; Miller, D. D.; Dalton, J. T.; Swaan, P. W. Structural determinants of P-glycoprotein-mediated transport of glucocorticoids. *Pharm. Res.* **2003**, *20*, 1794–1803.
- (23) Cerny, M. A.; Hanzlik, R. P. Cyclopropylamine inactivation of cytochromes P450: role of metabolic intermediate complexes. *Arch. Biochem. Biophys.* **2005**, *426*, 265–275.
- (24) Goncharov, N. V.; Jenkins, R. O.; Radilov, A. S. Toxicology of fluoroacetate: a review, with possible directions for therapy research. *J. Appl. Toxicol.* **2006**, *26*, 148–161.
- (25) van Niel, M. B.; Collins, I.; Beer, M. S.; Broughton, H. B.; Cheng, S. K. F.; Goodacre, S. C.; Heald, A.; Locker, K. L.; MacLeod, A. M.; Morrison, D.; Moyes, C. R.; O'Connor, D. O.; Pike, A.; Rowley, M.; Russell, M. G. N.; Sohal, B.; Stanton, J. A.; Thomas, S.; Verrier, H.; Watt, A. P.; Castro, J. L. Fluorination of 3-(3-(piperidin-1-yl)propyl)indoles and 3-(3-(piperazin-1-yl)propyl)indoles gives selective human 5-HT_{1D} receptor ligands with improved pharmacokinetic profiles. *J. Med. Chem.* **1999**, *42*, 2087–2104.
- (26) The absolute stereochemistry of **30** was proven by X-ray analysis, whereas the absolute stereochemistry at C3 and C4 of the piperidine ring in **31** is not known but is drawn as such to simplify visualization of the relative stereochemistry. See Experimental Section and Supporting Information for full details and characterization of all four isomers.
- (27) Crosio, C.; Fimia, G. M.; Loury, R.; Kimura, M.; Okano, Y.; Zhou, H.; Sen, S.; Allis, C. D.; Sassone-Corsi, P. Mitotic phosphorylation of histone H3: spatio-temporal regulation by mammalian aurora kinases. *Mol. Cell. Biol.* **2002**, *22*, 874–885.
- (28) Tao, W.; South, V. J.; Zhang, Y.; Davide, J. P.; Farrell, L.; Kohl, N. E.; Sepp-Lorenzino, L.; Lobell, R. B. Induction of apoptosis by an inhibitor of the mitotic kinesin KSP requires both activation of the spindle assembly checkpoint and mitotic slippage. *Cancer Cell* **2005**, *8*, 49–59.
- (29) In mouse models, MTD is typically defined as $\leq 10\%$ deaths due to mechanism-based toxicity. In studies with **30** infused at 12 (mg/kg)/day, there was 1 death out of 34 mice dosed, providing a 3% rate of death for this cohort.
- (30) The sequence of KSP is highly conserved across species, and the IC_{50} of **30** was found to be 2.2 ± 1.2 nM and 4.8 ± 1.0 nM against human and mouse KSP, respectively. Therefore, we expect little difference in therapeutic index across species due to differences in KSP potency.
- (31) For instance, compound **24** in ref 14 has cell potency and mouse shift numbers of 3.4 and 6.6 nM, respectively, and its in vivo EC_{90} is 38 nM.
- (32) Because mice become neutropenic and recover more quickly than humans, a once per week for 3 weeks schedule in humans ($q7d \times 3$) is mimicked by a once every 4 days for 12 days cycle in mouse ($q4d \times 3$). Minipumps were not used in this protocol to allow for dosing on multiple days.
- (33) Giannakakou, P.; Sackett, D. L.; Kang, Y.-K.; Zhan, Z.; Buters, J. T. M.; Fojo, T.; Poruchynsky, M. S. Paclitaxel-resistant human ovarian cancer cells have mutant β -tubulins that exhibit impaired paclitaxel-driven polymerization. *J. Biol. Chem.* **1997**, *272*, 17118–17125.
- (34) The data shown in Figure 4 for efficacy in the KB-v cell line were generated by dosing **30** on a $qd \times 1$ schedule at 40 mpk as a suspension in methylcellulose. This represents the MTD for this schedule, and this dosing paradigm has shown good efficacy in a number of experiments. The data from the $q4d \times 3$ schedule in the KB-v cell line are not shown because in this experiment (run only once), the vehicle control group displayed much less tumor progression than expected, similar to that of the group treated with **30**. However, as expected, the mice treated with paclitaxel in this study experienced significant tumor growth. The reason for the low rate of tumor progression in the vehicle group from this experiment is not known.
- (35) Yan, Y.; Sardana, V.; Xu, B.; Homnick, C.; Halczenko, W.; Buser, C. A.; Schaber, M.; Hartman, G. D.; Huber, H. E.; Kuo, L. C. Inhibition of a mitotic motor protein: where, how, and conformational consequences. *J. Mol. Biol.* **2004**, *335*, 547–554.
- (36) (a) Parish, C. A.; Adams, N. D.; Auger, K. R.; Burgess, J. L.; Carson, J. D.; Chaudhari, A. M.; Copeland, R. A.; Diamond, M. A.; Donatelli, C. A.; Duffy, K. J.; Faucete, L. F.; Finer, J. T.; Huffman, W. F.; Hugger, E. D.; Jackson, J. R.; Knight, S. D.; Luo, L.; Moore, M. L.; Newlander, K. A.; Ridgers, L. H.; Sakowicz, R.; Shaw, A. N.; Sung, C.-M. M.; Sutton, D.; Wood, K. W.; Zhang, S.-Y.; Zimmerman, M. N.; Dhanak, D. Novel ATP-competitive kinesin spindle protein inhibitors. *J. Med. Chem.* **2007**, *50*, 4939–4952. (b) Rickert, K. W.; Schaber, M.; Torrent, M.; Neilson, L. A.; Tasber, E. S.; Garbaccio, R. M.; Coleman, P. J.; Harvey, D.; Zhang, Y.; Yang, Y.; Marshall, G.; Lee, L.; Walsh, E. S.; Hamilton, K.; Buser, C. A. Discovery and biochemical characterization of selective ATP competitive inhibitors of the human mitotic kinesin KSP. *Arch. Biochem. Biophys.* **2008**, *469*, 220–231.
- (37) The coordinates have been deposited with the RCSB Protein Data Bank under the accession code 3CJO.
- (38) Stein, M. N.; Rubin, E. H.; Taber, K.; Fernandez, R. C.; Agrawal, N. G. B.; Vandrendreis, E.; Hsu, K.; Walker, A.; Holen, K.; Xue, L.; Cooley, P. C.; Wilding, G. Phase I clinical and pharmacokinetic (PK) trial of the kinesin spindle protein (KSP) inhibitor MK-0731 in patients with solid tumors. *J. Clin. Oncol.* **2007**, *25* (18S), 2548. (ASCO Annual Meeting Proceedings Part 1)
- (39) Shen, D. W.; Cardarelli, C.; Hwang, J.; Cornwell, M.; Richert, N.; Ishii, S.; Pastan, I.; Gottesman, M. M. Multiple drug-resistant human KB carcinoma cells independently selected for high-level resistance to colchicine, adriamycin, or vinblastine show changes in expression of specific proteins. *J. Biol. Chem.* **1986**, *261*, 7762–7770.

JM800386Y